

**THE IMBIBITION PROCESS OF WATERFLOODING IN NATURALLY
FRACTURED RESERVOIRS**

A Thesis

by

CHRISTIAN HUAPAYA LOPEZ

Submitted to the Office of Graduate Studies of
Texas A&M University
in partial fulfillment of the requirements for the degree of

MASTER OF SCIENCE

December 2003

Major Subject: Petroleum Engineering

**THE IMBIBITION PROCESS OF WATERFLOODING IN NATURALLY
FRACTURED RESERVOIRS**

A Thesis

by

CHRISTIAN HUAPAYA LOPEZ

Submitted to Texas A&M University
in partial fulfillment of the requirements
for the degree of

MASTER OF SCIENCE

Approved as to style and content by:

Robert A. Wattenbarger
(Chair of Committee)

David S. Schechter
(Member)

Brian J. Willis
(Member)

Hans C. Juvkam-Wold
(Head of Department)

December 2003

Major Subject: Petroleum Engineering

ABSTRACT

The Imbibition Process of Waterflooding in
Naturally Fractured Reservoirs. (December 2003)

Christian Huapaya López, B.S., National University of Engineering, Peru

Chair of Advisory Committee: Dr. Robert A. Wattenbarger

This thesis presents procedures to properly simulate naturally fractured reservoirs using dual-porosity models.

The main objectives of this work are to: (1) determine if the spontaneous imbibition can be simulated using a two phase CMG simulator and validate it with laboratory experiments in the literature; (2) study the effect of countercurrent imbibition in field scale applications; and (3) develop procedures for using the dual-porosity to simulate fluid displacement in a naturally fractured reservoir.

Reservoir simulation techniques, analytical solutions and numerical simulation for a two phase single and dual-porosity are used to achieve our objectives.

Analysis of a single matrix block with an injector and a producer well connected by a single fracture is analyzed and compared with both two phase single and dual-porosity models.

Procedures for obtaining reliable results when modeling a naturally fractured reservoir with a two phase dual-porosity model are presented and analyzed.

DEDICATION

This thesis is dedicated to:

My parents César and Alicia for their encouragement and motivation;

My brothers Osmand and César for their brotherhood.

ACKNOWLEDGMENTS

I would like to express my sincere gratitude and appreciation to Dr. Robert A. Wattenbarger for his assistance, encouragement and guidance throughout this research. It was his vision and experience which motivated me to complete this work.

Thank you to Drs. David Schechter and Brian Willis for serving as members of my graduate advisory committee.

I would also like to thank Mirko Hernandez, Fernando Changanqui, Kimberly Wolf, Carlos Hinostroza, Miguel De La Cruz, Marilyn Vilorio and Susanne Rustler for their valuable support, encouragement, advice and help in difficult times.

TABLE OF CONTENTS

	Page
ABSTRACT.....	iii
DEDICATION.....	iv
ACKNOWLEDGMENTS.....	v
TABLE OF CONTENTS.....	vi
LIST OF FIGURES.....	viii
LIST OF TABLES.....	x
CHAPTER	
I INTRODUCTION.....	1
1.1 The imbibition phenomenon.....	1
1.2 Background and motivation.....	1
II LITERATURE REVIEW.....	4
2.1 Introduction.....	4
2.2 Empirical transfer functions.....	4
2.3 Geometric factor methods.....	5
2.4 Modeling naturally fractured reservoirs.....	6
III SPONTANEOUS IMBIBITION.....	8
3.1 Spontaneous imbibition model.....	8
IV COMPARING ANALYTICAL SOLUTION WITH DETAILED MODEL.....	14
4.1 Introduction.....	14
4.2 Analytical formulation.....	14
4.3 Detailed model.....	16
4.4 Numerical simulation of detailed model.....	20
4.5 Comparison between analytical and numerical solution.....	22

CHAPTER	Page
V	COMPARING DETAILED MODEL WITH DUAL-POROSITY MODEL.... 25
5.1	Introduction..... 25
5.2	Dual-porosity formulations..... 25
5.3	Modeling dual-porosity..... 27
5.4	Comparing detailed model with dual-porosity model 29
5.5	Using pseudo-capillary pressure curve in the dual-porosity model..... 31
VI	DISCUSSION 34
6.1	General discussion 34
VII	CONCLUSIONS. 39
	NOMENCLATURE..... 40
	REFERENCES 42
	APPENDIX A..... 46
	VITA..... 55

LIST OF FIGURES

FIGURE	Page
3-1 Representation of 1-D spontaneous imbibition	9
3-2 Oil recovery for 1-D spontaneous imbibition	11
3-3 Water saturation profile for case A	12
3-4 Water saturation profile for case B	13
3-5 Water saturation profile for case C.....	13
4-1 Relative permeability and capillary pressure curves for matrix and fracture	17
4-2 Relative permeability curves for the fracture using Lantz's method	17
4-3 Schema of the fracture network of Spraberry	18
4-4 O'Daniel pilot area map and model to be simulated	19
4-5 Top view of an injector and a producer well connected by a single fracture	20
4-6 Comparison of water cut between the 51x11x1 and 51x25x1 models	21
4-7 Comparison of cumulative oil between the 51x11x1 and 51x25x1 models	21
4-8 Comparing water cut generated by De Swaan and detailed model.....	23
4-9 Comparing cumulative oil generated by De Swaan and detailed model.....	24
5-1 Top view of a scheme of a dual-porosity model	27

FIGURE	Page
5-2 Comparing water cut for 51x1x1 and 4x1x1 dual-porosity models.....	28
5-3 Comparing cumulative oil for 51x1x1 and 4x1x1 dual-porosity models.....	28
5-4 Top view of a scheme of the detailed and dual-porosity models.....	29
5-5 Comparing cumulative oil for detailed and dual-porosity models.....	30
5-6 Cumulative oil after applying pseudo-capillary pressure curve in the dual-porosity model	32
5-7 Cumulative produced water after applying pseudo-capillary pressure curve in the dual-porosity model.....	33
6-1 Scheme of half of the matrix's model	35
6-2 Water saturation profile in the matrix between injector and producer wells after 3 years for detailed and dual-porosity models.....	37
6-3 Water saturation profile in the matrix between injector and producer wells after 6 years for detailed and dual-porosity models.....	37
6-4 Water saturation profile in the matrix between injector and producer wells after 9 years for detailed and dual-porosity models.....	38

LIST OF TABLES

TABLE		Page
3-1	Properties of rock and fluids	10
4-1	Properties of rock and fluid of Spraberry	16
6-1	Comparing the average water saturation in the matrix block for detailed and dual-porosity model after 3 years	35
6-2	Comparing the average water saturation in the matrix block for detailed and dual-porosity model after 6 years	36
6-3	Comparing the average water saturation in the matrix block for detailed and dual-porosity model after 9 years	36

CHAPTER I INTRODUCTION

1.1 Imbibition phenomenon

Imbibition plays an important role in recovering oil from water-wet matrix in a naturally fractured reservoir subjected to waterflood.

Using the action of capillary forces, it allows the recovery of oil within the matrix blocks that cannot be reached by the external pressure gradients during waterflood. Capillary pressure is a function of capillary radius, interfacial tension, and wettability of the rock.

Imbibition is an immiscible displacement process, whereby a fluid which is within a porous medium is spontaneously expelled by another fluid surrounding the medium. This phenomenon results from differential attraction forces between the pore walls and the fluids.

Spontaneous countercurrent imbibition, in which water and oil flow through the same face in opposite directions, is a dominant mechanism for the exchange between matrix and fractures in water-wet rocks. In spontaneous imbibition, wetting fluid is drawn into rock by capillary suction as the non-wetting fluid is expelled.

1.2 Background and motivation

A naturally fractured reservoir is a porous rock formation in which stress have created planar discontinuities that either positively or negatively affect fluid flow by 1) increasing reservoir permeability 2) increasing porosity, and/ or 3) increasing permeability anisotropy.

Fractured sandstone reservoir rock contains two porosity systems; 1) intergranular void spaces between the grains of the rock have high porosity and low permeability, and 2) fractures have low porosity and high permeability, typically greater an order of magnitude greater permeability from between the intergranular pores.

Secondary porosity is the porosity created by post-genetic processes as fracturing and dissolution. Dual-porosity is the combination of the two. Both primary and secondary porosity are progressively destroyed as sediments are buried, mainly by processes of cementation and compaction. Typically, intergranular pores store most of the fluids (90 percent) whereas fractures act as transmission channels through the fracture.

Numerous hydrocarbon reservoirs in the world are naturally fractured. Estimating the efficiency of water injection processes in recovering hydrocarbons from these reservoirs remain complicated by poor knowledge of fracture network geometry and production behavior of the matrix blocks in contact with water along fractures.

De Swaan¹ and Mattax and KYTE² investigated the mechanism of countercurrent imbibition and developed relationships describing cumulative oil recovery versus time. The work validates these equations by numerical simulations at both laboratory and field size scales.

Naturally fractured reservoirs are simulated using both single and dual porosity models, assuming a continuum, matrix and fractures within each grid block. Dual-porosity models deal with transfer coefficients and shape factor related with dimension of matrix blocks surrounded by the wetting fluid. Two-phase single and dual-porosity models are compared and procedures for simulating naturally fractured reservoirs undergoing waterflood properly are proposed.

When performing numerical simulation of naturally fractured reservoirs using dual-porosity model there is uncertainty in the results of this model due to different finite difference formulations. Dual-porosity model assumes that the matrix blocks are instantaneously immersed in water, which is the main factor for discrepancy in production.

Results will be used for simulating naturally fractured reservoirs properly using dual-porosity model for field scale.

CHAPTER II

LITERATURE REVIEW

2.1 Introduction

Empirical transfer functions deal primarily with fluid flow interaction between the matrix and the fracture. Flow interaction between matrix and fracture is what happens in a naturally fractured reservoir undergoing waterflood. Geometric shape factors are related with the geometry of matrix block considering the fracture spacing in each direction. The last section focused on modeling naturally fractured reservoirs.

2.2 Empirical transfer functions

De Swaan¹ presented a theory of waterflooding in naturally fractured reservoirs for the case of two incompressible fluids. This theory accounts for varying water saturations in fractures that occur when water is injected in naturally fractured reservoirs. De Swaan compared results of his theory with numerical simulations of Kleppe and Morse².

Matax and Kyte³ studied the one-dimension and three-dimension spontaneous imbibition in alundum and sandstone cores of different lengths with fluids of various viscosity were used in the experiments. The time required to recover a given fraction of oil from matrix pores was related to the square of the distance between fractures. In these experiments, carried out as static imbibition, core samples were surrounded with static brine. A critical rate was defined as the rate at which water advance in the fracture equals that in the matrix block. The laboratory experiments were up scale to full field dimensions applying Rapoport's laws.

Aronofsky⁴ assumed an exponential equation to describe the exchange of oil and water for a single matrix block initially saturated with oil and completely immersed in water. Kazemi⁵ developed an analytical solution of the Buckley-Leveret displacement in a fracture surrounded by matrix block undergoing imbibition. Results are similar to de Swaan's.

2.3 Geometric factor methods

Warren and Root⁶ models a fractured reservoir formed by identical rectangular parallelepipeds separated by an orthogonal network of fractures. For this model only two parameters are sufficient to characterize a naturally fractured reservoir, one parameter relating fluid capacitance of the secondary porosity and the other relating the scale of heterogeneity in the system. The model assumes interporosity flows occur under pseudo-steady state conditions.

Gilman and Kazemi⁷ developed a much more realistic model that considers matrix blocks of variable lengths. They presented two-phase dual- porosity simulator, in which the matrix/fracture transfer coefficients include gravity forces. Gravity potential between matrix and fracture nodes is addressed. Their shape factor was calculated as

$$\sigma = 4 \left(\frac{1}{L_x^2} + \frac{1}{L_y^2} + \frac{1}{L_z^2} \right) \quad (1)$$

L_x, L_y, L_z are the matrix block dimensions.

Rangel and Kovscek⁸ derived a time dependent shape factor considering varying filling and instantly filled matrix block. The shape factor was shown to vary with time. However, the shape factor in commercial simulators is erroneously considered constant.

Thomas *et al*⁹ developed a fully implicit three-phase model simulator for naturally fractured reservoirs based on an extension of the matrix/fracture transfer function of Warren and Root and accounts for gravity, capillary pressure and viscous forces.

Bourblaux and Kalaydjian¹⁰ executed laboratory experiments of cocurrent and countercurrent imbibition occurring in a single block of a strongly water-wet matrix and tested them with a numerical model. As relative permeability curves are determined for cocurrent flow the use of these for countercurrent should be different. Numerical simulation suggested that relative permeability curves for oil and water should be reduced by a factor of 30% in order to agree with experimental results.

Gurpinar and Kossack¹¹ performed numerical simulation with a core plug grid size for a single porosity model and compared it with a fine and coarse grid blocks for dual- porosity model. Fracture width used in the simulation runs was 0.1 ft, which is too big and not representative for natural fracture in a reservoir. Also, the pseudo capillary pressure was used in the dual porosity model in order to match it with the solution of their single porosity model.

Lee and Kang¹² modeled fracture aperture heterogeneity using statistic analysis and analyzed the oil recovery of the fractured cores undergoing water injection using these statistic parameters.

2.4 Modeling naturally fractured reservoirs

Single porosity models predict flow through a continuous media and can be used to predict fluid behavior through a single block in naturally fractured reservoirs. Impractical when the numbers of fractured blocks applied to an entire field for the numbers of grid blocks.

Naturally fractured reservoir performance can be managed with dual-porosity models, which define two set of properties such as porosity and permeability per grid block, one for the matrix system and the other for the fracture system. In a dual-porosity model movement is assumed to occur between matrix blocks and fractures. Some models of the matrix/ fracture system geometry are presented as Warren⁶ and Gilman and Kazemi⁷. The flow of fluids through the reservoir occurs through the fracture system.

The main difference between the dual-permeability model and the standard dual porosity model is that the movement of fluids can be between matrix-matrix and fracture-fracture flow between the simulation grid blocks.

CHAPTER III

SPONTANEOUS IMBIBITION

If a core is totally immersed in water, water will be absorbed and oil will be released. Spontaneous countercurrent imbibition is the principal mechanism for the exchange of fluids between matrix and fractures. In spontaneous imbibition the flow of oil and water occurs in contrary directions over the same face of a matrix block. The rate of imbibition depends on wettability of the rock¹³, pore structure, interfacial tension, viscosity, initial water saturation and relative permeabilities¹⁴.

Therefore, a good understanding of this physical process will tremendously improve the modeling of fluid flow in naturally fracture systems.

3.1 Spontaneous imbibition model

In this case we are simulating a core in which only one face is exposed to water and the others are covered with plastic. So in this way we are simulating spontaneous imbibition in only one-dimension.

Fig. 3-1 represents a core with one side exposed to water and shows the pressure distribution along the system one moment before the imbibition starts. The pressure of the oil in the core zone is the pressure of the whole system both water and core zone. The pressure of the water in the core zone is lower than the pressure of oil due to the capillary pressure in the porous media at initial conditions.

Simulation runs were compared with the laboratory experiments of Mattax and KYTE³. They concluded that the time to recover certain amount of oil depends on the distance between the fractures and the scale equation is expressed in the following way

$$\left(t \sqrt{\frac{k}{\phi} \frac{\sigma 1}{u_w L^2}} \right)_{\text{model}} = \left(t \sqrt{\frac{k}{\phi} \frac{\sigma 1}{u_w L^2}} \right)_{\text{matrixblock}} \quad (2)$$

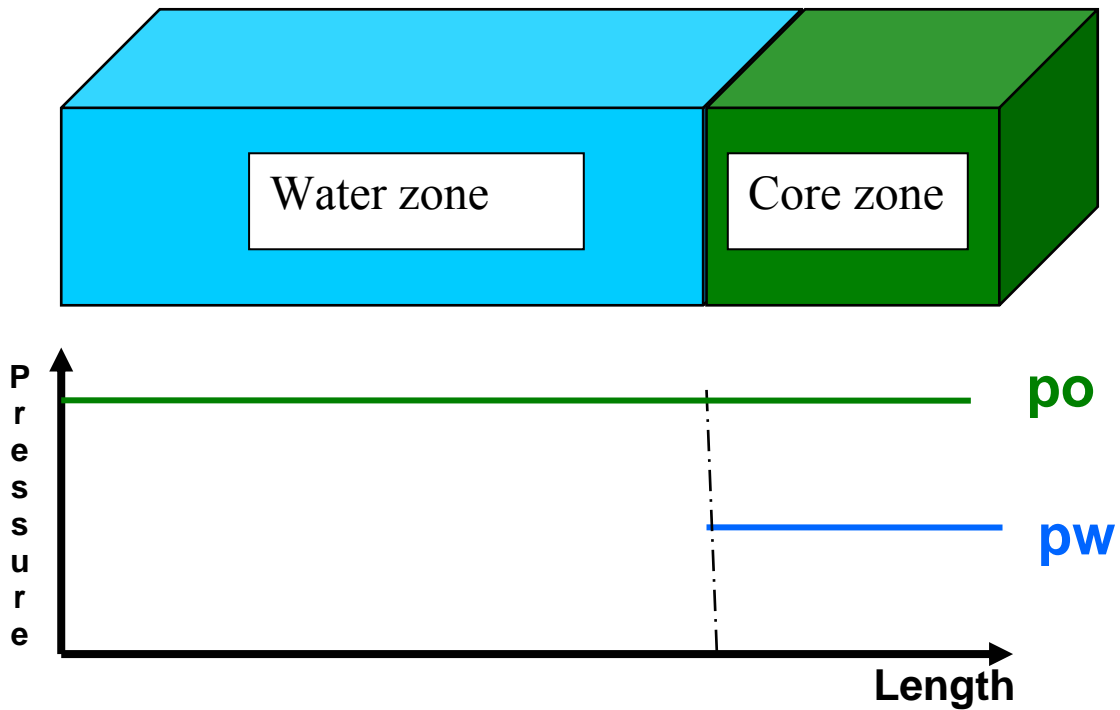


Fig. 3-1 – Representation of 1-D spontaneous imbibition.

Parallelepiped shapes maintaining the same cross-area and the same length were modeled as the cores because the CMG simulator cannot model the cylindrical shapes of the actual cores. Mattax and Kyte conducted laboratory experiments not only for different viscosities of oil and water but also for different lengths of the alundum core. The properties of these alundum cores for the cases A, B and C are shown in **Table 3-1**.

Table 3-1 – Properties of rock and fluid

Case	Sample Length (cm)	Sample Area (cm ²)	Dry Air Permeability (darcies)	Porosity (%)	Oil Viscosity cp	Water Viscosity cp	Oil-Water Inter. Tension (dyne/cm)
A	5.08	11.36	1.475	29.1	8.5	0.9	35
B	11.049	11.36	1.545	28.3	8.5	0.9	35
C	11.049	11.36	1.545	28.3	121.8	12.9	36

Fig. 3-2 shows oil recovery from the cores. Dots show the laboratory data and line the numerical simulation. Values of relative permeabilities and capillary pressure curves were assumed in order to match simulation with the experimental results. The water zone was modeled with one grid block with a high value of permeability of 10 darcy and a value of porosity of 100%. In addition, the cores were modeled with very fine grid blocks next to water zone and with coarser grid blocks as they are getting further from the water zone.

The plot demonstrates that countercurrent flow and spontaneous imbibition can be simulated with the CMG simulator.

A water saturation profile along the cores for different times is plotted for the three cases.

Fig. 3-3 shows the case A, which has a core length of 5.08 cm. It can be seen that after 60 minutes of water imbibition, the water saturation in the face of the core has not great difference with the one at the end of the core. This is because the water imbibing the core takes short time to reach the other end of the core. Also, an average water saturation of 84% is within the core, which is reached after 200 minutes and most of the movable oil has moved to the water zone.

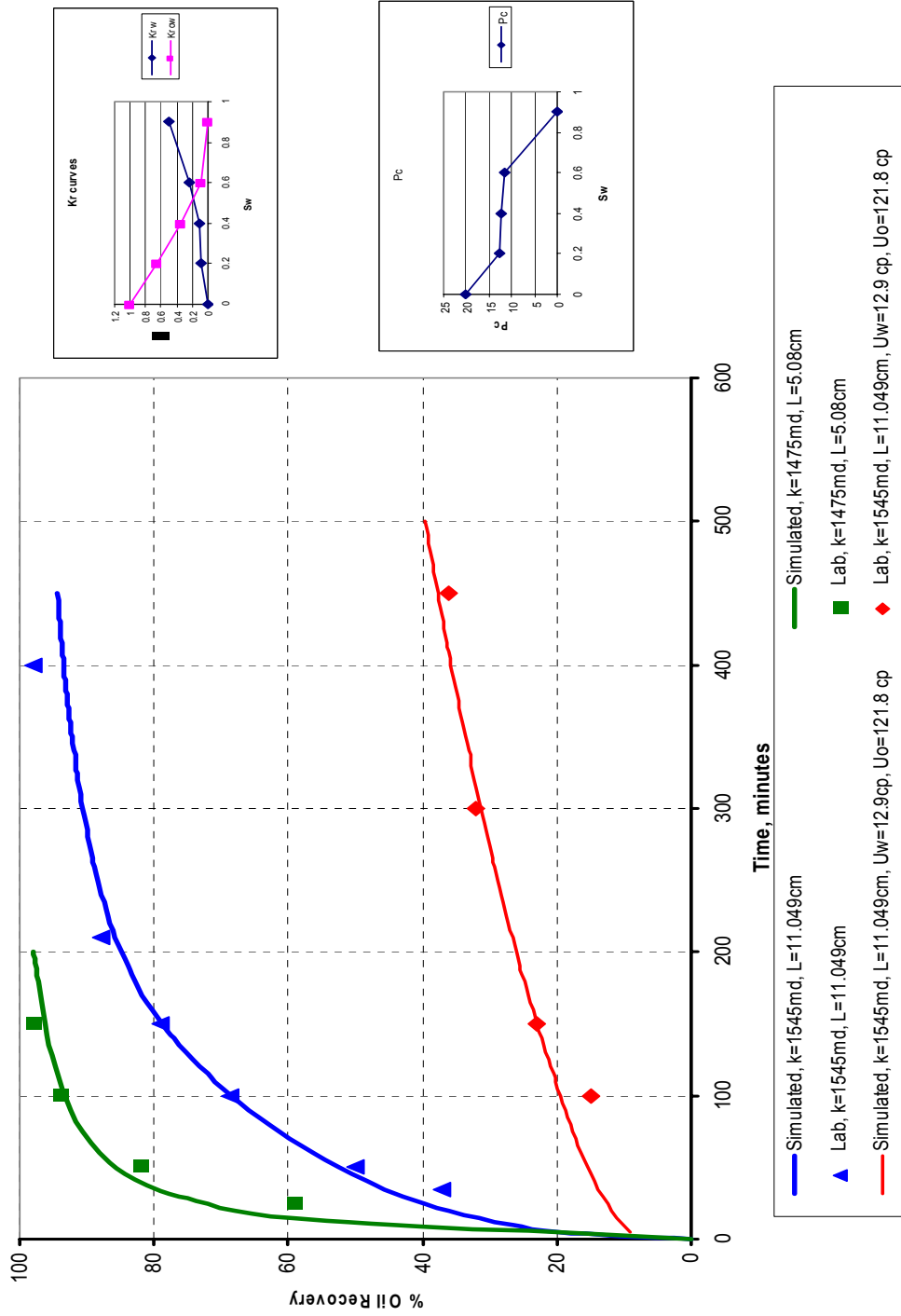


Fig. 3-2 – Oil recovery for 1-D spontaneous imbibition.

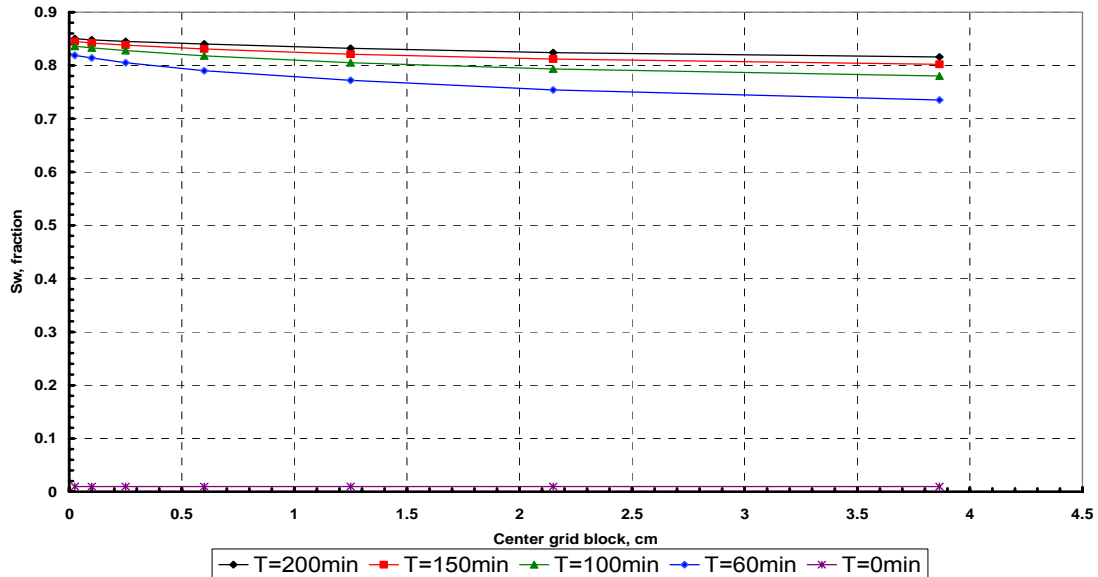


Fig. 3-3 – Water saturation profile for case A.

Figs. 3-4 and **Fig. 3-5** show cases B and C respectively, both cases have the same core length of 11.05 cm and same permeability, the only difference between the two cases is that the viscosities of the oil and the water are higher but maintaining the same viscosity ratio of 9.4 in both cases. In case B the water imbibes the core faster than in case C, this is due to higher viscosities of the fluids and the restricted countercurrent flow. As can be noticed the water at the end of the core has rarely felt the presence of water. Also, comparing case B and C, it is easily determined that the viscosities of the fluids are very important in the recovery of spontaneous imbibition.

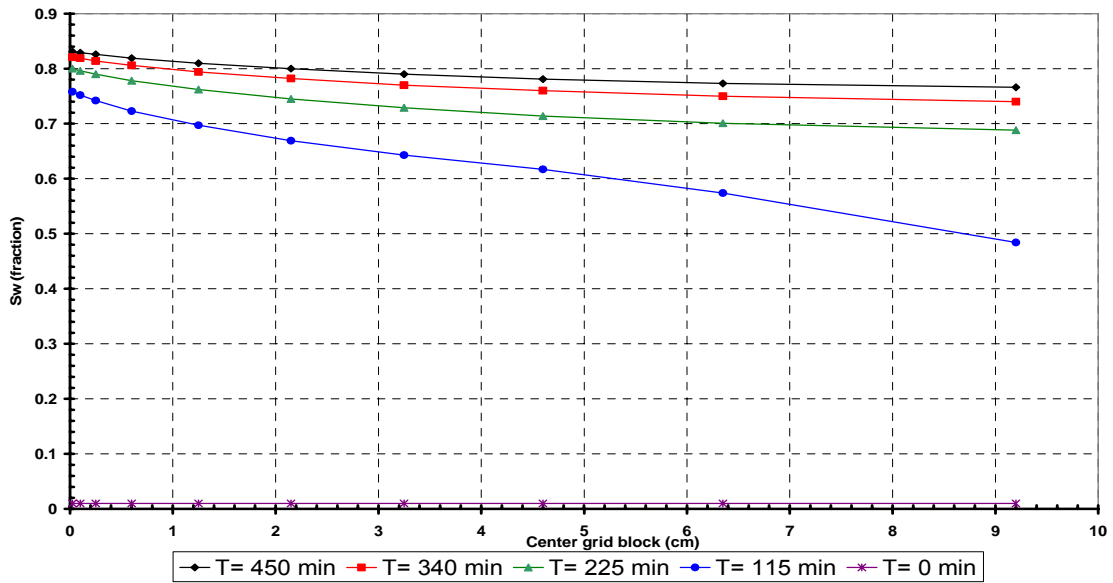


Fig. 3-4 – Water saturation profile for case B.

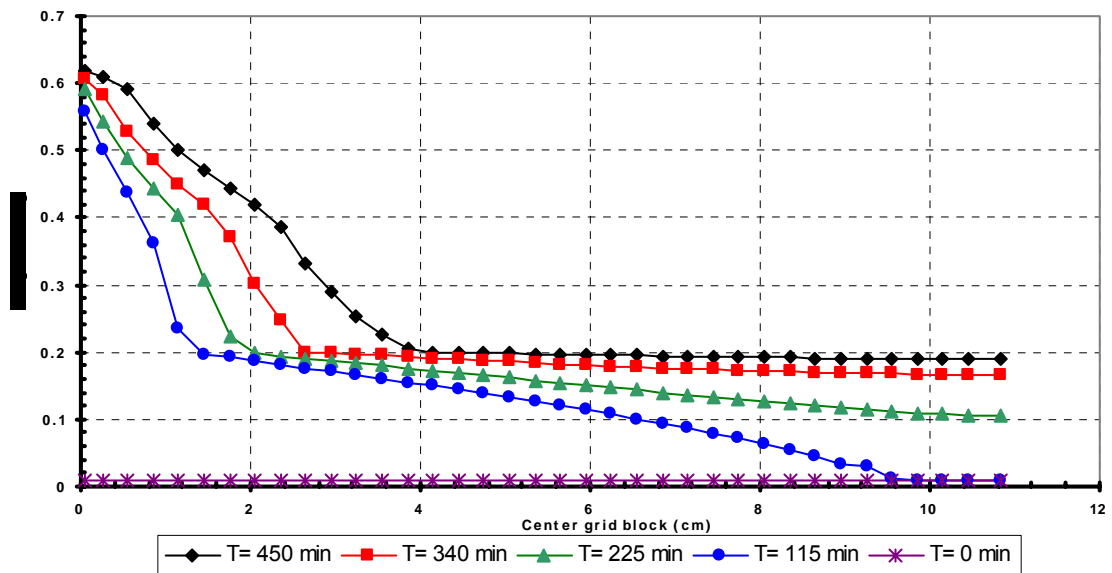


Fig. 3-5 – Water saturation profile for case C.

CHAPTER IV

COMPARING ANALYTICAL SOLUTION WITH DETAILED MODEL

4.1 Introduction

Numerical simulation of naturally fractured is difficult due to the difficulty in predicting fracture networks and exchange of fluids between matrix and fracture systems.

Several papers discuss the matrix/fracture transfer function^{1,3,5,15,16}. Mostly of them assumed that the fracture is instantaneously immersed in water. However, De Swaan assumed varying water saturation through the fracture.

In this chapter a comparison between a 2-D single porosity model (detailed model) and De Swaan's formulation is presented.

4.2 Analytical formulation

Aronofsky's model assumed that the matrix is instantaneously submerged in water. Aronofsky predicted that

$$R = R_{\infty}(1 - e^{-\lambda t}) \quad (3)$$

Where λ is a fitting parameter and R_{∞} is the ultimate cumulative oil recovery from the imbibition process. It can also be expressed in the following way.

$$q = \frac{R_{\infty}}{\tau_1} e^{-t/\tau_1} \quad (4)$$

However, De Swaan's model supposed that water saturation through the fracture is varying with time. This model represents when water is injected into the fracture and imbibes the matrix block progressively until reach the producer well.

The following was assumed in this model;

- 1) Water tends to advance in high-transmissibility fractures. The water in the fracture is absorbed as it advances and time passes. Besides that, the water in the fracture is imbibed into the matrix and the matrix releases an equivalent amount of oil.
- 2) If a matrix block is immersed totally in water, it will absorb water and release oil at a rate exponential (Aronofsky). The rate of water imbibition per unitary fracture length is given by.

$$q_{lu} = \frac{R_{\infty u}}{\tau_1} \int_0^t e^{-(t-\theta)/\tau_1} \frac{\partial S_w}{\partial \theta} d\theta \quad (5)$$

- 3) The continuity equation in a lineal reservoir is given by

$$-\frac{\partial q_w}{\partial x} = h_f \phi_{fe} \frac{\partial S_w}{\partial t} + \frac{R_{\infty u}}{\tau_1} \int_0^t e^{-(t-\theta)/\tau_1} \frac{\partial S_w}{\partial \theta} d\theta \quad (6)$$

- 4) The fractional flow of every phase is identical with the phase's mobile saturation

$$f_j = S_j \quad (7)$$

$$-\frac{\partial q_w}{\partial x} = h_f \phi_{fe} \frac{\partial S_w}{\partial t} + \frac{R_{\infty u}}{\tau_1} \int_0^t e^{-(t-\theta)/\tau_1} \frac{\partial S_w}{\partial \theta} d\theta \quad (8)$$

For different time necessary to inject the fracture's mobile volume at constant injection rate (t_{if})

For $t < t_{if}$

$$S_w = 0 \quad (9)$$

$$Np = i_w t \quad (10)$$

For $t > t_{if}$

$$S_w = 1 - e^{-t/\tau_1} \int_0^{t_{if}/\tau_1} e^{-y} I_0(2\sqrt{ty/\tau_1}) dy \quad (11)$$

$$N_p = i_w \int_{t_{if}}^t e^{-\theta/\tau_1} \int_0^{t_{if}/\tau_1} e^{-y} I_0(2\sqrt{\theta y/\tau_1}) dy d\theta \quad (12)$$

4.3 Detailed model

A numerical simulation of a 2-D single porosity model (detailed model) was used assuming rock and fluid properties of Spraberry trend area¹⁷. This area is located in the Midland Basin, a geological province of the Permian Basin, in West Texas. The pay-depth is at about 7000-8000 ft, and consists of fine-grained sandstones, coarse siltstones, and organic rich shales.

The areas of Spraberry have signs of having natural fractures. Core analysis and well logs show that the matrix has permeability order of 0.05 md and porosity 6 to 14 percent. Effective permeability obtained from buildup tests, step rate injection range from 1 to 200 md¹⁷.

Table. 4-1 and **Fig. 4-1** show the properties of Spraberry.

Table 4.1- Properties of rock and fluid of Spraberry.

Matrix Porosity	0.1
Matrix Permeability (md)	0.1
Fracture permeability (md)	17000
Fracture aperture (ft)	0.00108
Initial pressure (psi)	2300
Water viscosity (cp)	0.51
Oil viscosity (cp)	1.3

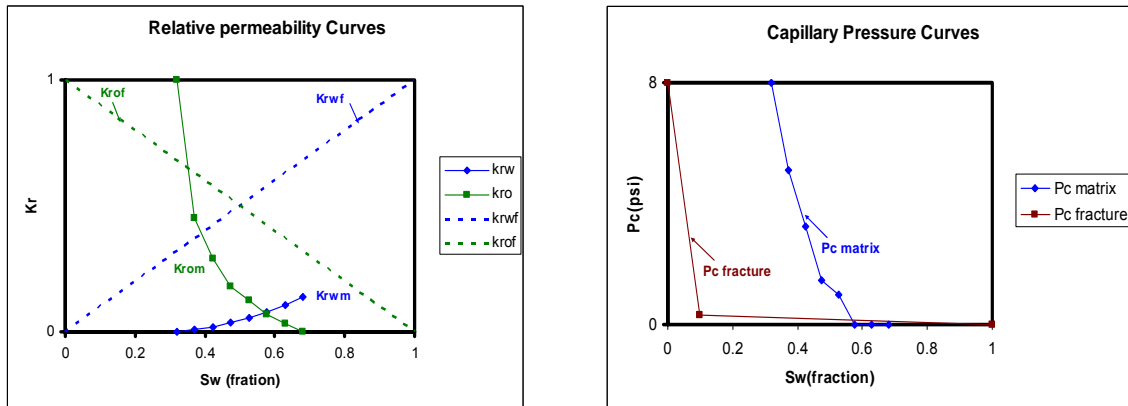


Fig. 4-1 –Relative permeability and capillary pressure curves for matrix and fracture.

For simplicity, the relative permeabilities used in the fracture were assumed to be straight lines, which mean that relative permeabilities are equal to their respective saturations see **Fig. 4-1**. Lantz¹⁸ shows how to calculate relative permeabilities that should be used in an immiscible simulator to model this type of process. **Fig. 4-2** represents the relative permeability curves according to Lantz's equations for this model with the conditions of viscosity of oil and water of 1.3 cp. and 0.51cp. respectively. The relative permeabilities in **Fig. 4-2** were not used in this work but should be used in future work.

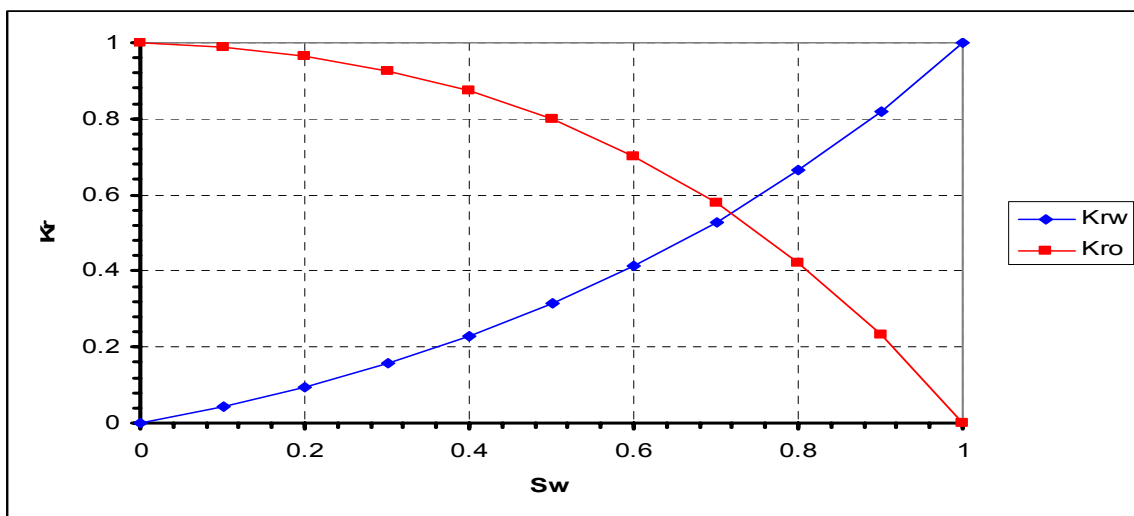


Fig. 4-2 –Relative permeability curves for the fracture using Lantz's method.

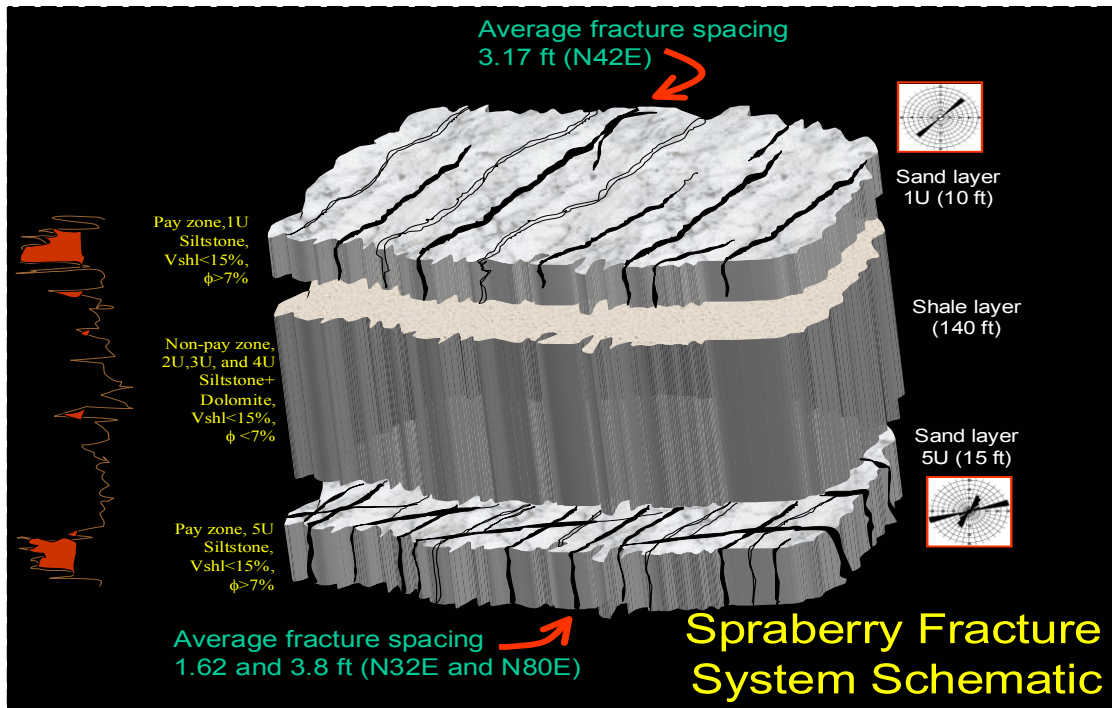


Fig. 4-3 –Schema of the fracture network of Spraberry (after Schechter).

The formation is subdivided into the Lower, Middle and Upper Spraberry members. Only, units 1U and 5U from the upper Spraberry give significant production. A schema of the fracture network for Spraberry is shown in **Fig. 4-3**.

Fig. 4-4 Pilot of waterflood pattern in the O’Daniel area used to create a simulation model composed of one producer well and one injector connected for a single fracture.

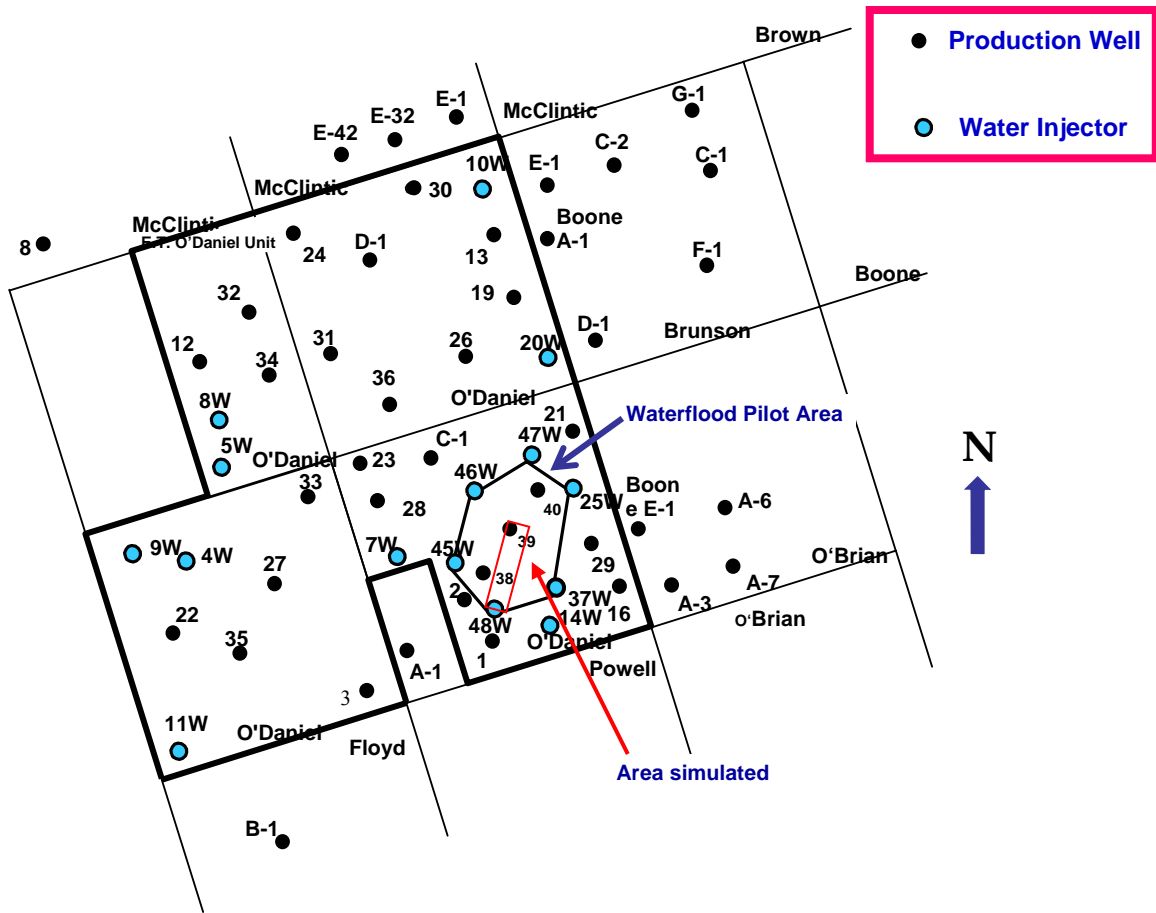


Fig. 4-4 –O’ Daniel pilot area map and model to be simulated.

Fig. 4-5 model to be simulated: injector and producer well connected by a single fracture in a single matrix block. Fracture spacing is 3.17 ft. and a formation thickness is 10 ft, averages values for 1U unit in the Spraberry area. Injector and a producer are separated 1060ft, which is approximately the distance between the wells 48W and 39.

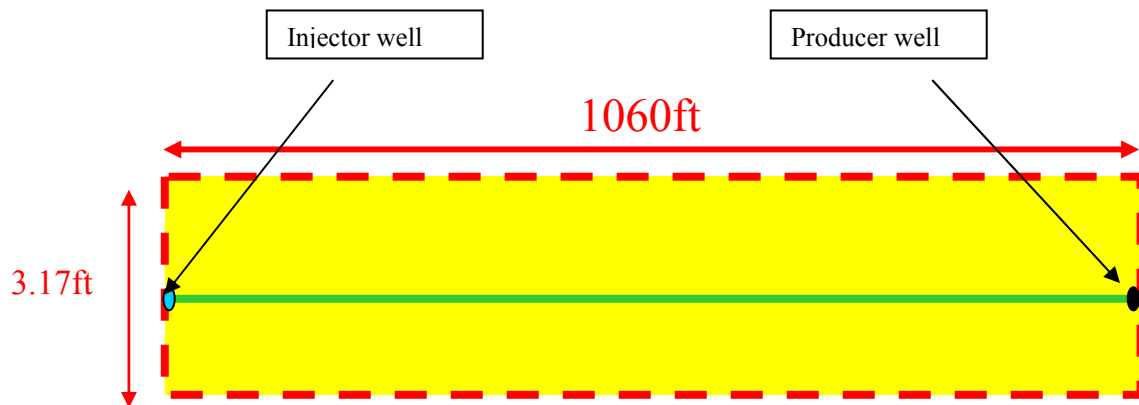


Fig. 4-5 – Top view of an injector and producer well connected by a single fracture.

4.4 Numerical simulation of detailed model

A single porosity model was built with a commercial simulator. The Spraberry is a very tight formation, and thus can be assumed that there is no flow in the matrix. Therefore, the fluid produced from the producer well comes from the flow through the fracture.

Fig. 4-5 is modeled with 51x11x1 number of grid blocks of. This model was compared with another one with a number of grid blocks of 51x25x11, making it finer in the direction parallel to the fracture. The comparison of water cut and cumulative oil plot between the two models are shown in **Fig. 4-6** and **Fig. 4-7** respectively. Both models fine and coarse in the fracture spacing direction match perfectly.

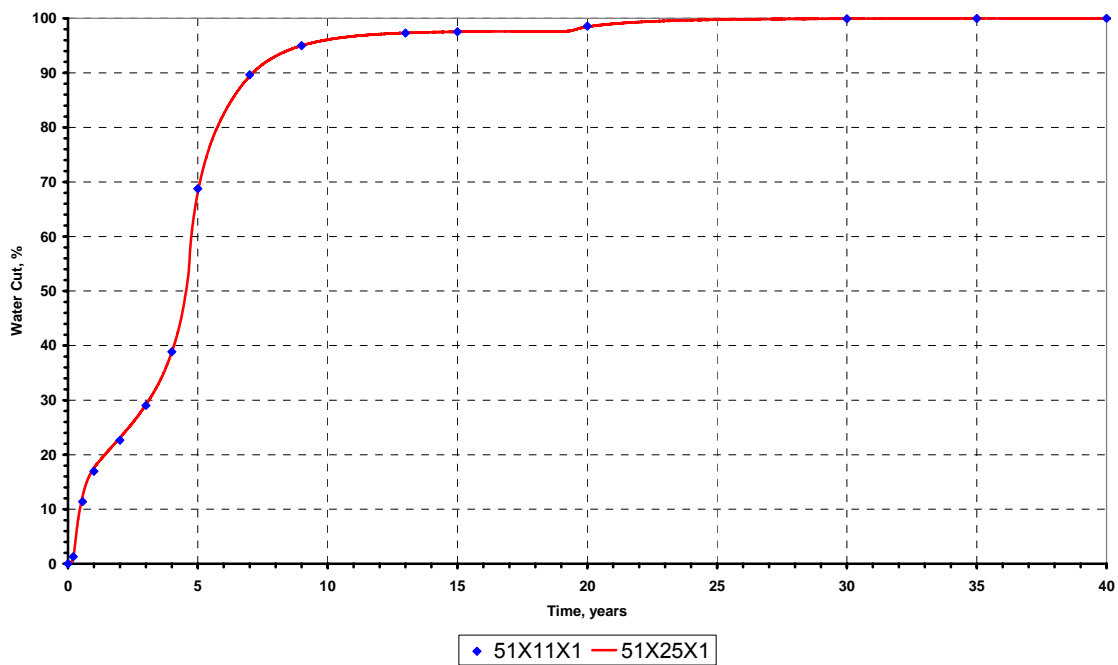


Fig. 4-6 – Comparison of water cut between the 51x11x1 and 51x25x1 models.

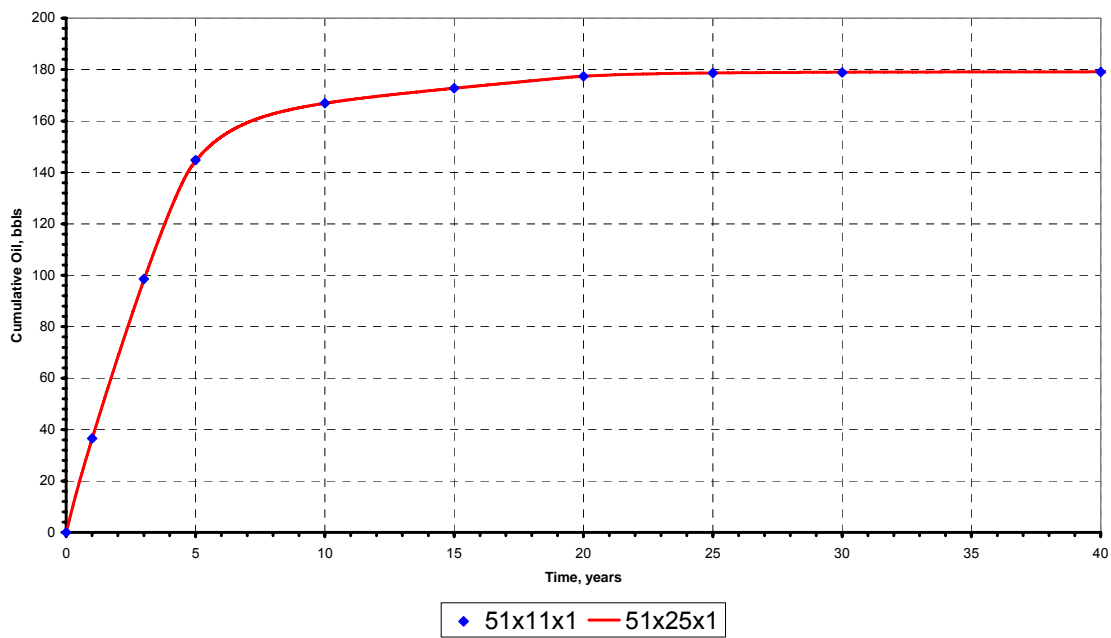


Fig. 4-7 – Comparison of cumulative oil between the 51x11x1 and 51x25x1 models.

In both models the water injected is equal to the amount of fluid recovered from the producer well, in this case the maximum constant water injection that this model can maintain is 0.1 bbl/d. This constrain was established in order to compare it with the De Swaan solution. The total movable oil in the model is 217.6 bbls, which means that a recovery of 82.7 percent is obtained after 25 years. Most of the recovery, 67.2 percent is obtained in the first five years due to countercurrent flow. In addition, another model of 101x11x1 was compared with the one of 51x11x1 showing exactly the same results. This means that a base model of 51x11x1 is very representative.

4.5 Comparison between analytical and numerical solution

In order to use De Swaan's equations values of t_{if} and the time necessary to inject the matrix recoverable oil volume at i_w (t_{iN}) are determined

$$t_{if} = \frac{xh_f \phi_{fe}}{i_w} \quad (13)$$

$$t_{iN} = \frac{xR_{\infty H}}{i_w} \quad (14)$$

The value of t_{iN} obtained is 6 years and the value of t_{if} was considered zero because the pore volume of the fracture is very small compared with the pore volume of the matrix block. As the imbibition constant (τ_1) is unknown, it was adjusted to match with the results of the detailed model. A very acceptable match is presented in **Fig. 4-8** and **Fig. 4-9** for a value of τ_1 of 1.5.

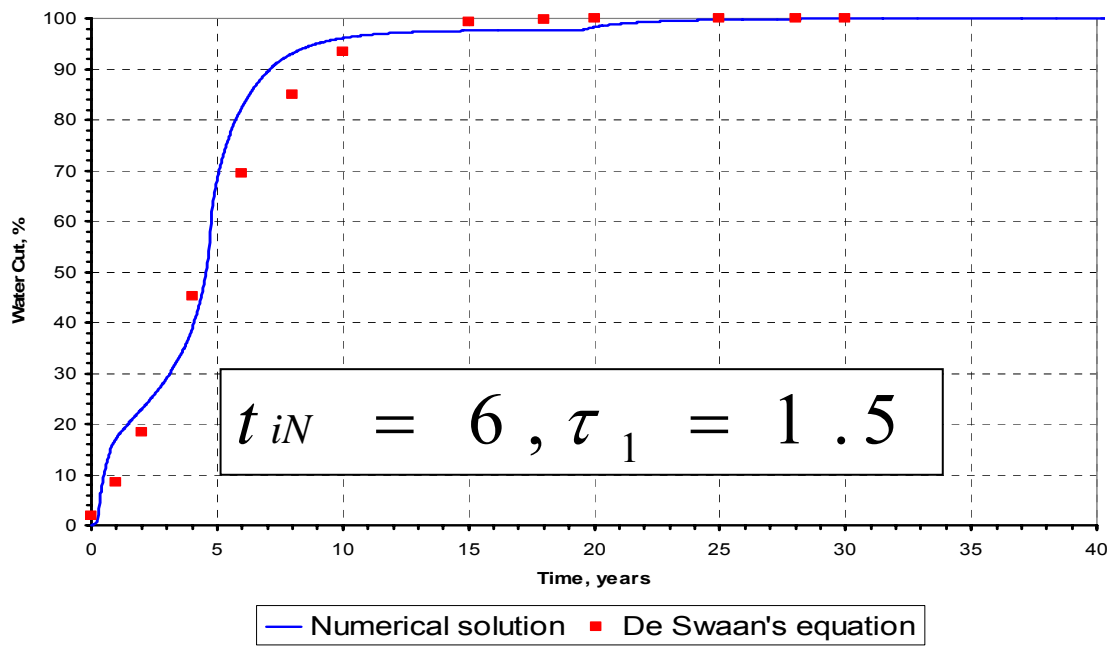


Fig. 4-8 – Comparing water cut generated by De Swaan and detailed model.

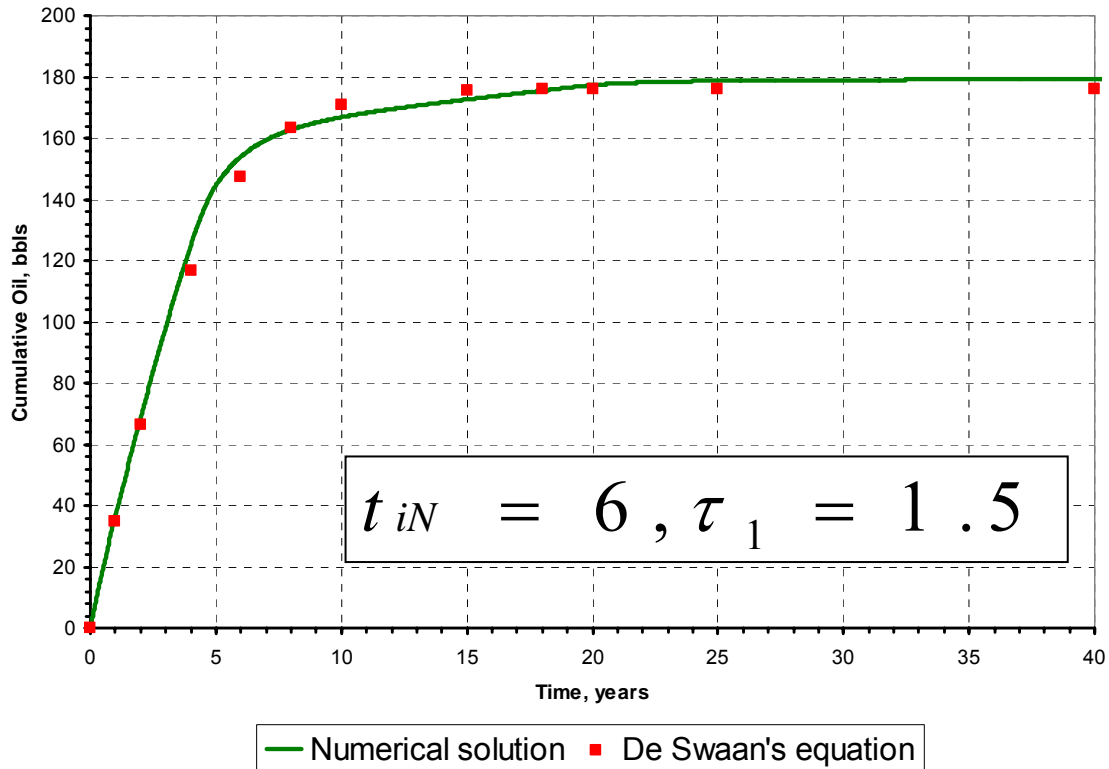


Fig. 4-9 – Comparing cumulative oil generated by De Swaan and detailed model.

The Swaan's formulation can also be used for field scaled models when determining t_{iN} and calibrating τ_1 with a previous simulation result.

CHAPTER V

COMPARING DETAILED MODEL WITH DUAL POROSITY MODEL

5.1 Introduction

Naturally fractured reservoirs are probably the most complex of all the reservoir systems. The orientation, width, spacing and permeability are necessary to describe the fractures network. All of the mentioned above but the permeability determines the geometry of the matrix block. The determination of a matrix/fracture system for modeling a dual porosity system is very difficult.

A single matrix block can be simulated using a single porosity simulator with fine grid blocks¹⁹. However, this method is not practical when doing field scale simulation of a naturally fractured reservoir.

Commercial numerical models can manage flow of fluids in naturally fractured reservoir. However, the results of those may not be representatives. In commercial dual-porosity and dual-permeability simulators, the interporosity flow rate is proportional to the shape factor, which is assumed to be a constant value considering the geometry of the matrix block.

In this chapter, some procedures for getting reliable results when modeling naturally fractured reservoirs undergoing waterflood using dual porosity models are given.

5.2 Dual-porosity formulations

In dual porosity models the fluid flow in each grid block is only between matrix and fracture. The finite difference equations for dual porosity models developed by Gilman and Kazemi⁷ and used by CMG²⁰ simulator for oil and water are the following.

For fracture

$$\Delta [T_{cf}(\Delta p_{cf} - g_{cf}\Delta D_f)] - T_{cma}[(p_{cf} - g_{cf}D_f) - (p_{cma} - g_{cma}D_{cma})] + q_\alpha = \frac{V_b}{\Delta t} \Delta_t \left(\frac{\phi S_\alpha}{B_\alpha} \right)_f \quad (15)$$

For matrix

$$T_{ama} [(p_{cf} - g_{cf} D_f) - (p_{ama} - g_{ama} D_{ama})] = \frac{V_b}{\Delta t} \Delta_t \left(\frac{\phi S_\alpha}{B_\alpha} \right)_{ma} \quad (16)$$

The transfer of the fracture, T_{cf}

$$T_{cf} = 0.001127 \left(\frac{k k_{ra} \phi}{u_\alpha B_\alpha} \right)_f \left(\frac{\Delta y \Delta z}{\Delta x} \right) \quad (17)$$

The transfer of the matrix, T_{ama}

$$T_{ama} = .001127 k_{ma} \Delta x \Delta y \Delta z \sigma \left[\omega \left(\frac{k_r}{uB} \right)_{ma} + (1 - \omega) \left(\frac{k_r}{uB} \right)_f \right] \quad (18)$$

The shape factor, σ

$$\sigma = 4 \left(\frac{1}{L_x^2} + \frac{1}{L_y^2} + \frac{1}{L_z^2} \right) \quad (19)$$

In **Eq. 18** ω is an upstream weighting factor. When ω is one, flow is from matrix to fracture and when zero flow is from fracture to matrix. T_{ama} relies on the transfer of water between matrix and fracture. If the term T_{ama} is canceled the finite difference equation for the fracture in **Eq. 16** is the same as the equation for a single porosity. This term depends directly of the shape factor σ , and assuming that the whole matrix block is instantaneously immersed in water.

5.3 Modeling dual-porosity

Several papers discuss modeling dual-porosity^{21,22,23,24,25}. As we want to compare a detailed model with a dual porosity model for a single matrix block, we will construct a dual-porosity model with the same properties. That is fracture spacing is 3.17 ft., distance between the wells is 1060 ft and rock-fluid properties are those in **Table 4.1**. **Fig. 5-1** shows a scheme of the one dimension dual porosity model.

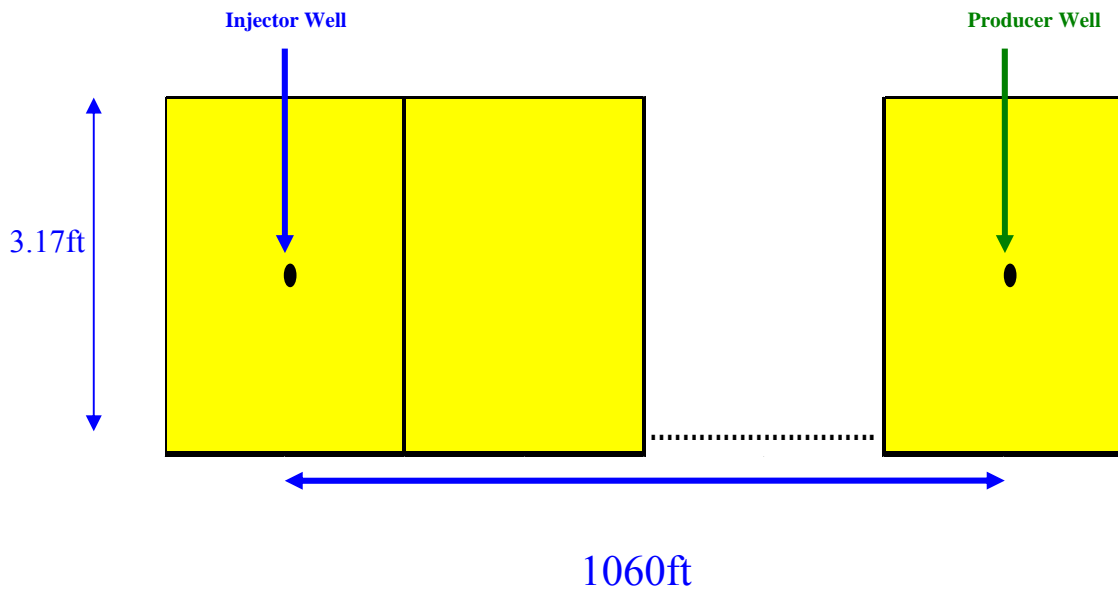


Fig. 5-1 – Top view of a scheme of a dual-porosity model.

Grid block sensitivity is performed to determine the minimum number of grid blocks that can be used with no great difference in the performance results. Models with 51x1x1, 26x1x1, 11x1x1, 4x1x1 grid block were simulated. Comparison between the finest and coarsest grid block models of water cut and cumulative oil are shown in **Fig. 5-2** and **Fig. 5-3** respectively.

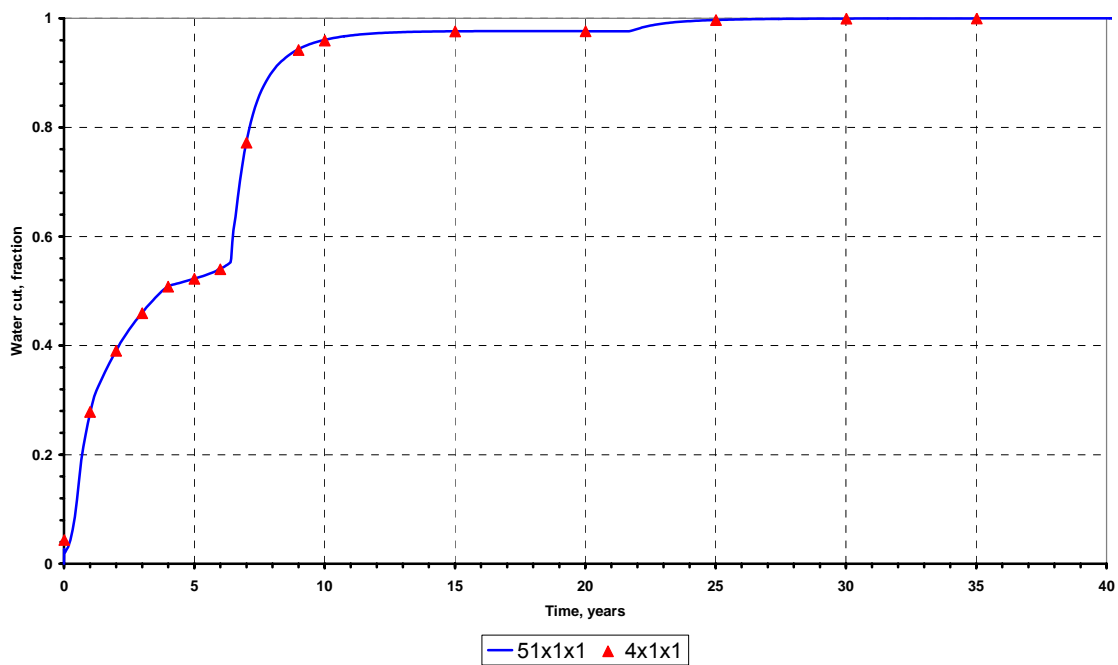


Fig. 5-2 – Comparing water cut for 51x1x1 and 4x1x1 dual-porosity models.

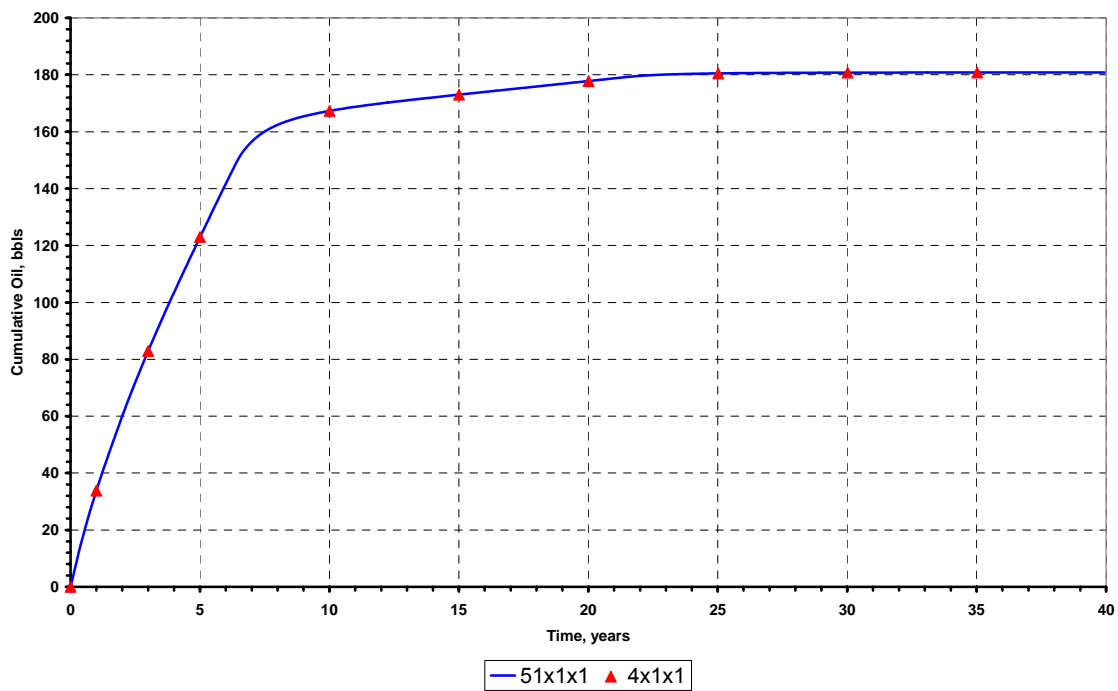


Fig. 5-3 – Comparing cumulative oil 51x1x1 and 4x1x1 dual-porosity models.

It can be easily seen that the finer and coarser grid block give exactly the same results. This means that for this case, the dual-porosity model is not sensitive to the grid block size and that the refinement of the grid blocks in a dual-porosity simulation has no effect in the performance of fluid displacement. This also means that modeling with the coarse one dimension dual-porosity model uses less computational time than the detailed model, give same performance and is cheaper computationally.

5.4 Comparing detailed model with dual-porosity model

After doing grid block sensitivity analysis between the detailed dual-porosity models, now the next step is to compare both models, the results from the detailed model are considered the solutions, in **Fig. 5-4** shows both model to be compared.

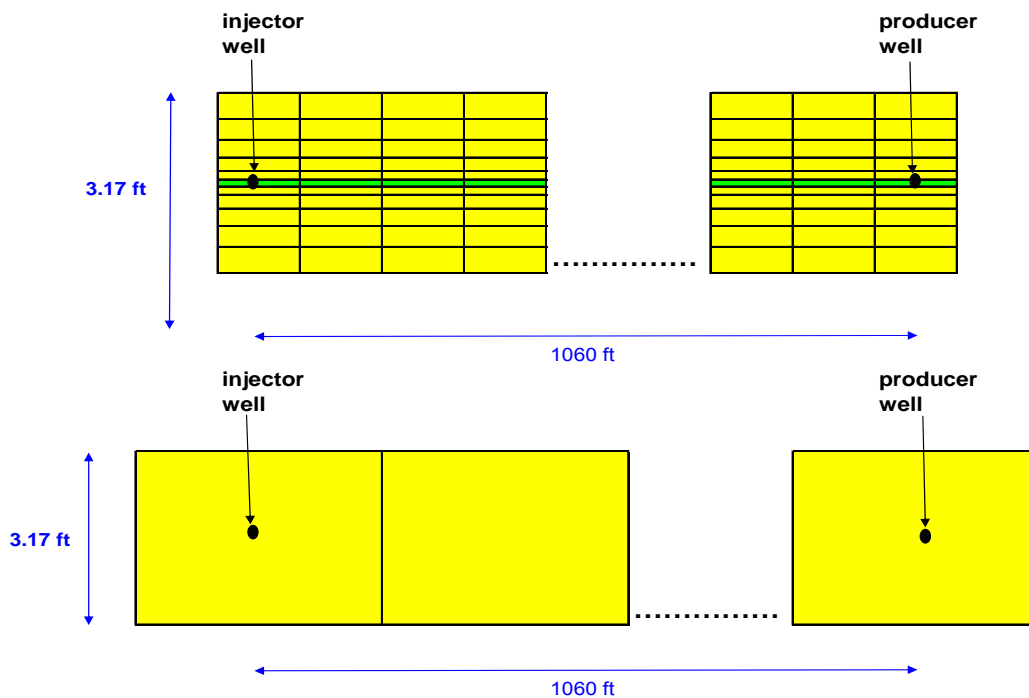


Fig. 5-4 – Top view of a scheme of the detailed and dual-porosity models.

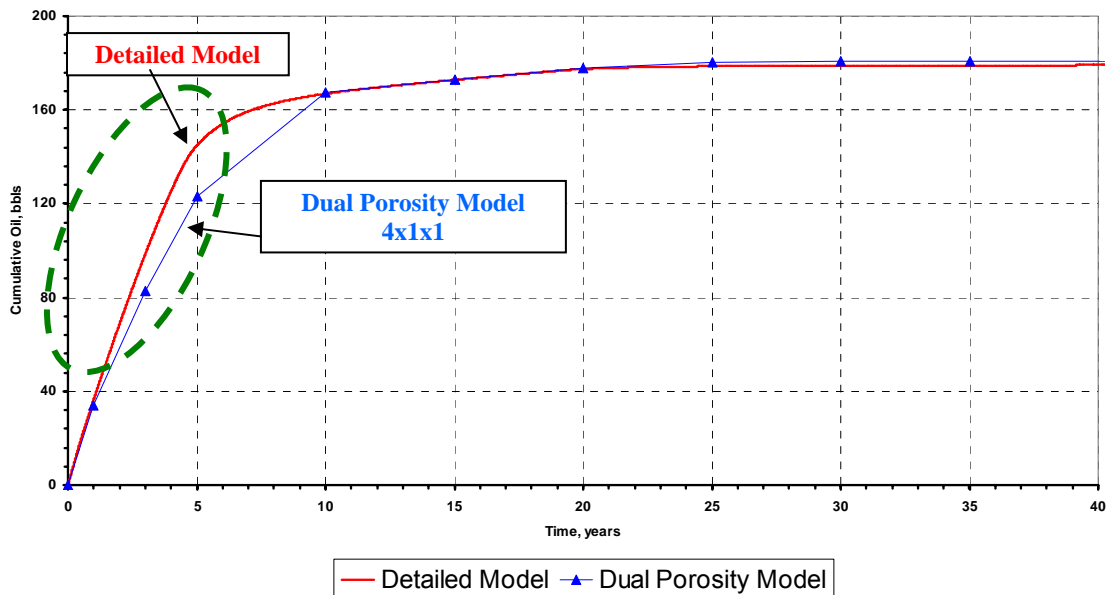


Fig. 5-5 – Comparing cumulative oil for detailed and dual-porosity models.

Fig. 5-5 Cumulative oil curve calculated with the dual-porosity model doesn't match the detailed model. This discrepancy is because the shape factor in the CMG simulator doesn't take into account partially immersed fractures, and assume constant shape factor. A constant shape factor is not realistic because matrix block cannot be assumed in contact with the wetting phase⁸ all the time; in these two models the fracture is filled with oil at initial conditions and experiences a varying water saturation of the fracture as time passes. The cumulative oil at the beginning doesn't match, the cumulative oil is considerable low and after ten years both cumulative oil curves match.

5.5 Using pseudo-capillary pressure curve in the dual-porosity model

One attempt to match the detailed model with the dual-porosity model was to increase the value of the transfer of water between the matrix block and the fracture system. This can be performed by increasing the shape factor, which means to reduce the fracture spacing. However, when reducing the fracture spacing more parallel fractures within the same matrix block appears and the volume of the matrix system is reduced and consequently the volume of the fracture system is increased. This method is not considered because is not physically the same as the detailed model in **Fig. 5-4**. In addition, when increasing the shape factor two completely different models are being modeled.

Based on the scaling laws given by Rapoport and applied in some other papers^{3,11}, an increase in the capillary pressure curve was performed maintaining the same values of connate water saturation and residual oil saturation. **Table 5-1** shows the original values of capillary pressure and the pseudo capillary pressures used for matching the detailed model.

Table 5-1 Capillary pressure curves for detailed model and dual-porosity model

Sw	Pc original (psi)	Pc match (psi)
0.32	8	200
0.371429	5.10346	60
0.422857	3.23304	10
0.474286	1.48148	1.8
0.525714	1	1
0.577143	0	0
0.628571	0	0
0.68	0	0

Fig. 5-6 and **Fig. 5-7** show the match after applying the pseudo capillary pressure curve in the dual-porosity model. When trying to match the detailed model with values of capillary pressure higher of 200 psi no significant improvement was observed.

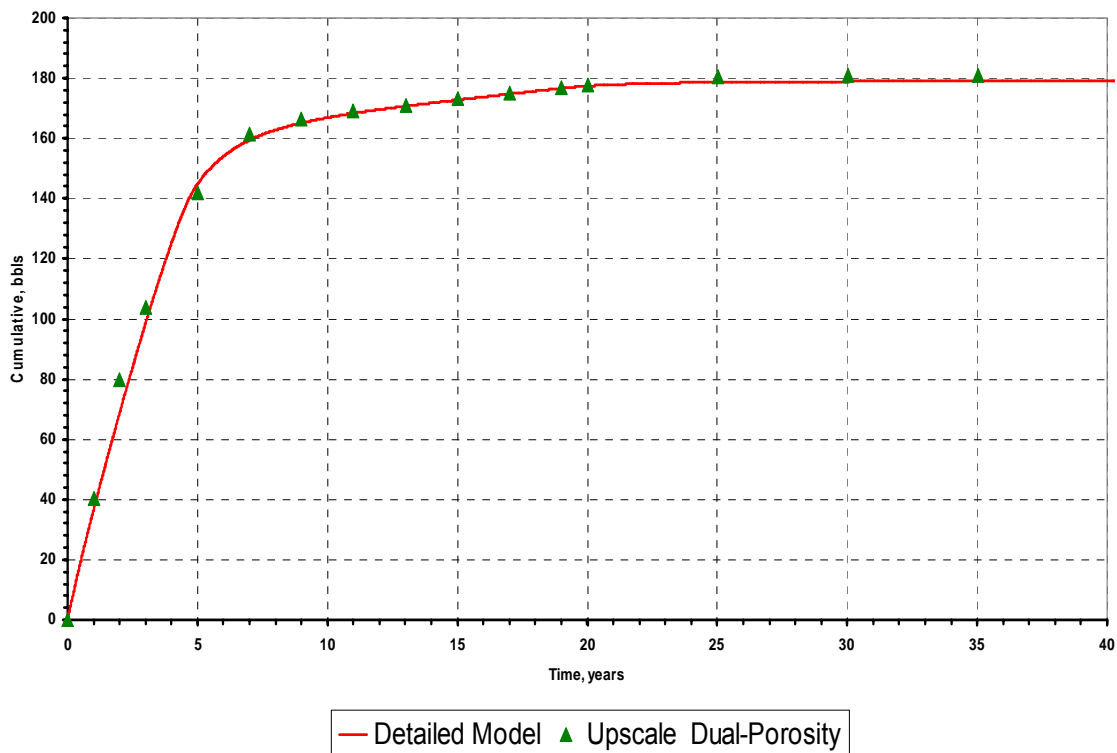


Fig. 5-6 – Cumulative oil after applying pseudo-capillary pressure curve in the dual-porosity model.

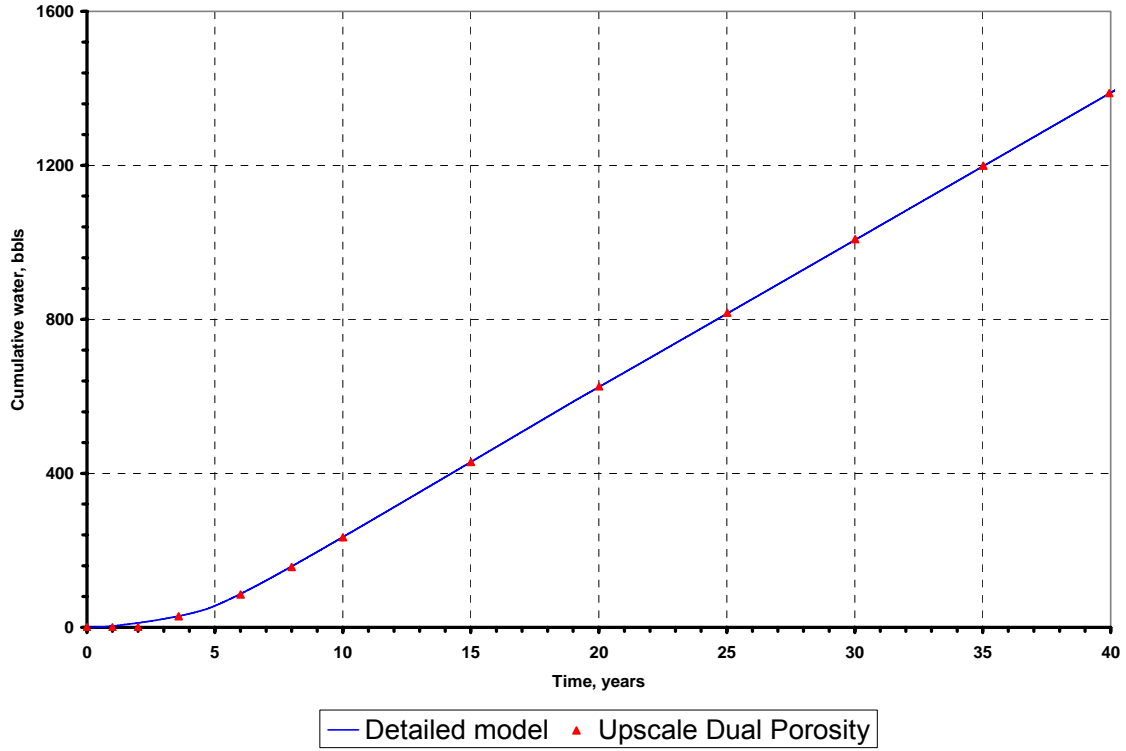


Fig. 5-7 – Cumulative produced water after applying pseudo-capillary pressure curve in the dual-porosity model.

CHAPTER VI

DISCUSSION

6.1 General discussion

A valid match between the detailed and dual-porosity model after using a pseudo capillary pressure curve was obtained. Cumulative oil and produced cumulative water were matched. The only distance points between the producer and the injector wells, where there is a coincidence between the centers of the grid block are the ones where the two wells are located. Therefore, the average water saturations in the matrix for different times is determined in these locations.

Fig. 6-1 represents a scheme of the injector and producer wells and the zones where the average water saturations are determined.

Table 6-1, Table 6-2 and Table 6 -3 show the average water saturation for the detailed and dual-porosity models. The value of the average water saturation for the dual-porosity model was obtained directly from the output file of this model. However, for determining the average water saturation for the detailed model (51x11x1) the values of water saturation in the center of each grid block that represent the matrix, in this case only five grid blocks due to the symmetry of the model. In addition, the average water saturation for the detailed model was determined volumetrically.

In the dual-porosity model the average matrix water saturations for the grid blocks where the wells are located shows small differences compared with its equivalent detailed model. This happen because the CMG simulator doesn't take into account a varying shape factor with time, which accounts for partially water immersed fractures. Instead, it assumes a shape factor that is constant all the time, which is not realistic.

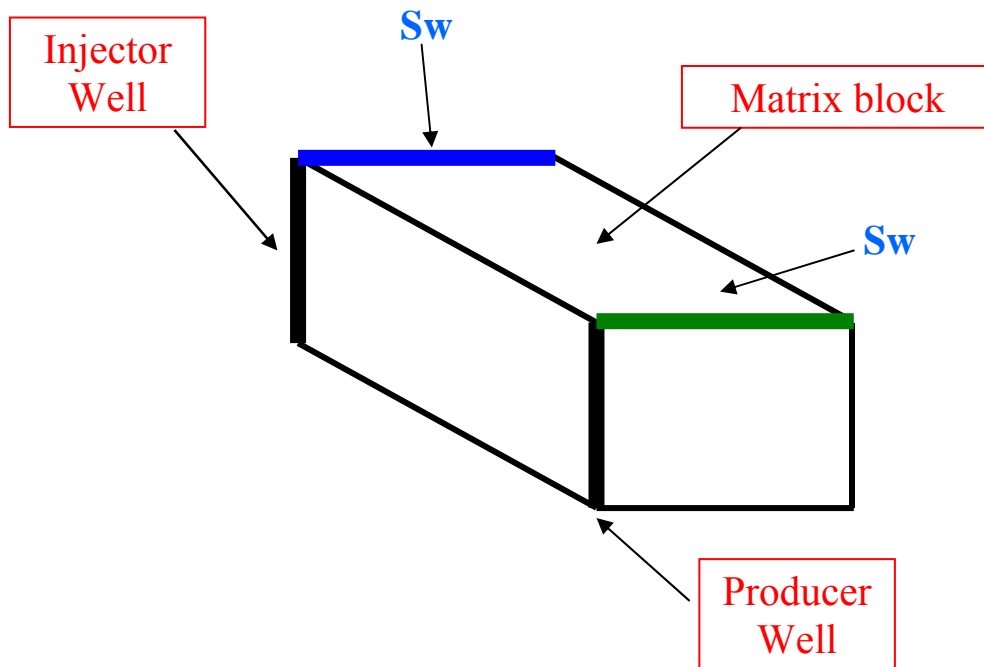


Fig. 6-1 – Scheme of half of the matrix’s model.

Fig. 6-2, **Fig. 6-3** and **Fig. 6-4** show the water saturation profile in the matrix for both models. The three cases show a very acceptable match along the wells

Table 6-1 Comparing the average water saturation in the matrix block for detailed and dual-porosity model after 3 years

	Water saturation along the injector well for detailed model	Water saturation along the producer well for detailed model
	0.541	0.35
	0.553	0.358
	0.565	0.364
	0.574	0.368
	0.576	0.369
Average Sw for detailed model	0.551	0.351
Average Sw for dual-porosity model	0.489	0.478

Table 6-2 Comparing the average water saturation in the matrix block for detailed and dual-porosity model after 6 years

	Water saturation along the injector well for detailed model	Water saturation along the producer well for detailed model
	0.566	0.509
	0.57	0.537
	0.574	0.555
	0.576	0.568
	0.577	0.573
Average Sw for detailed model	0.569	0.528
Average Sw for dual-porosity model	0.566	0.558

Table 6-3 Comparing the average water saturation in the matrix block for detailed and dual-porosity model after 9 years

	Water saturation along the injector well for detailed model	Water saturation along the producer well for detailed model
	0.572	0.563
	0.574	0.567
	0.576	0.571
	0.577	0.574
	0.577	0.575
Average Sw for detailed model	0.574	0.566
Average Sw for dual-porosity model	0.574	0.572

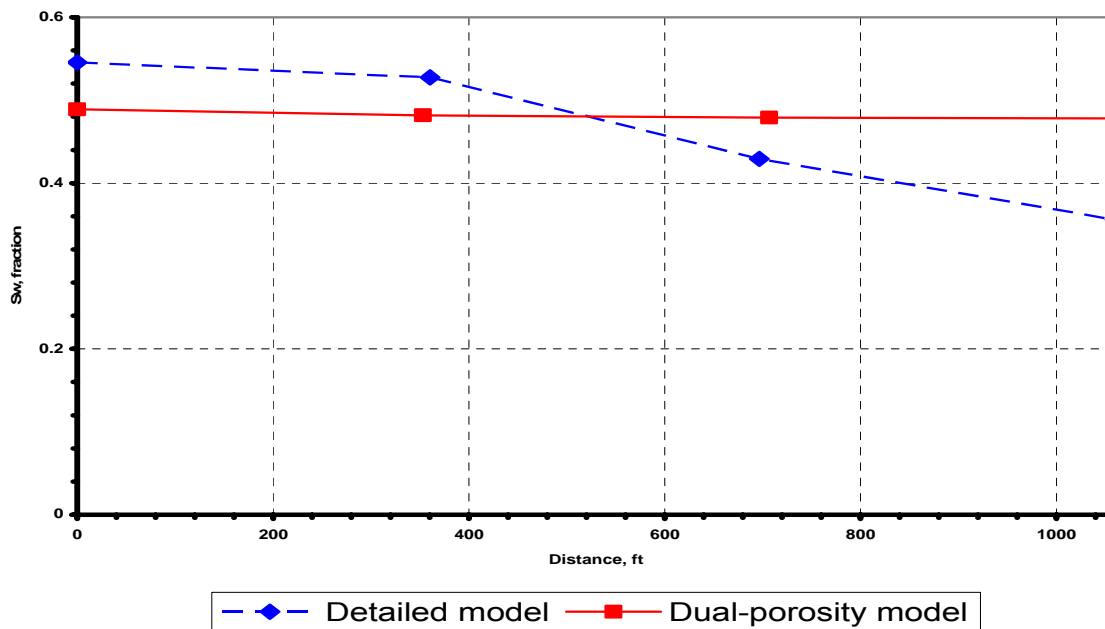


Fig. 6-2 – Water saturation profile in the matrix between injector and producer wells after 3 years for detailed and dual-porosity models.

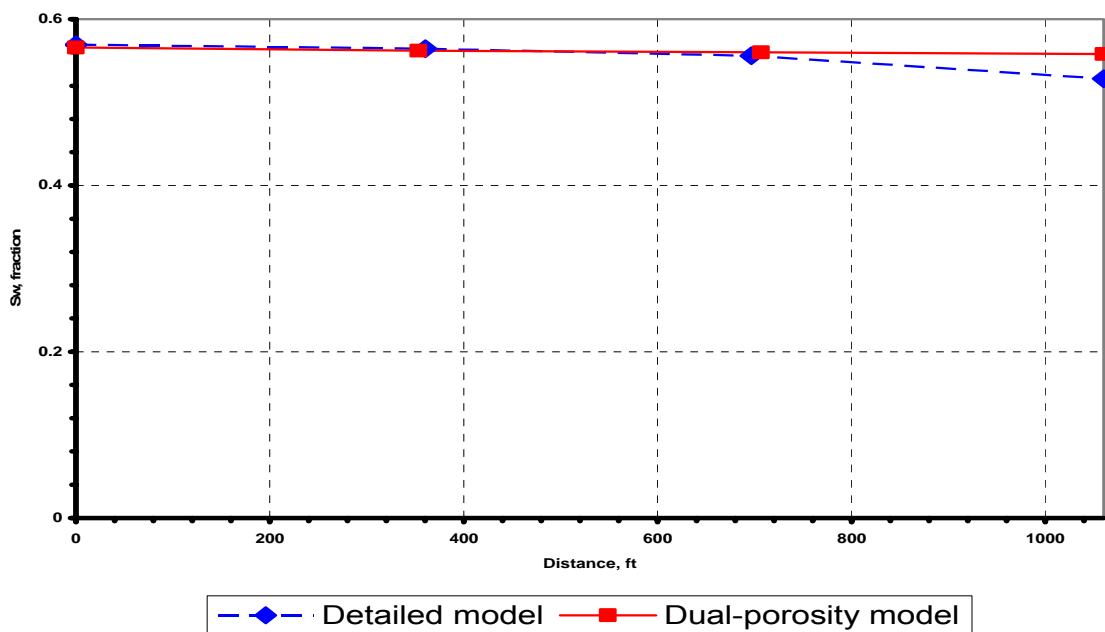


Fig. 6-3 – Water saturation profile in the matrix between injector and producer wells after 6 years for detailed and dual-porosity models.

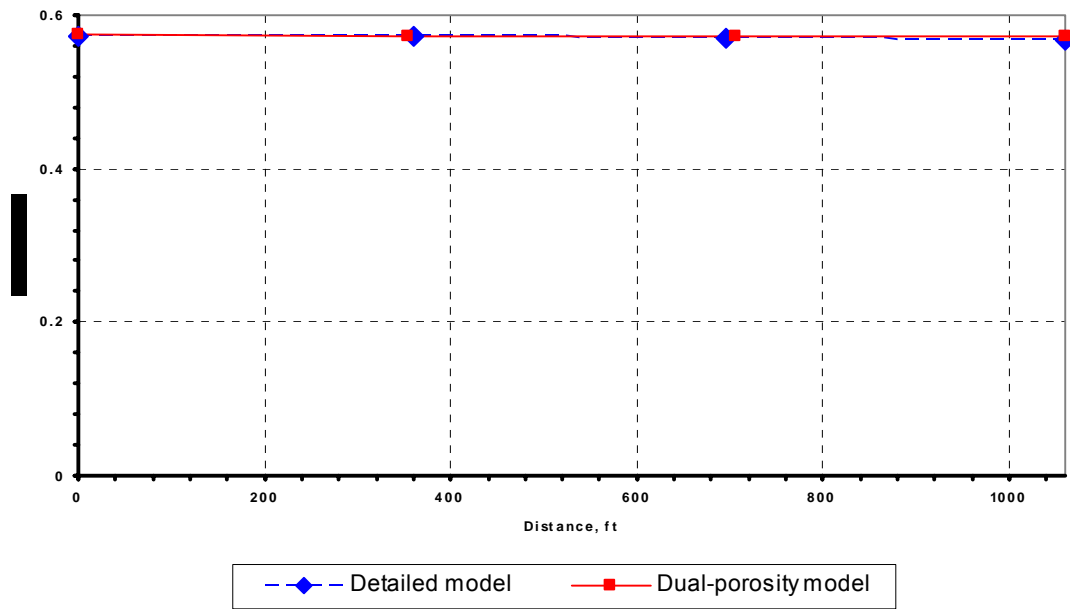


Fig. 6-4 – Water saturation profile in the matrix between injector and producer wells after 9 years for detailed and dual-porosity models.

CHAPTER VII

CONCLUSIONS

A method described to simulate properly naturally fractured reservoir undergoing waterflood is described. The following conclusions can be drawn based on this research work:

1. The following procedures are used to simulate a fractured matrix grid block.
 - a) Estimate the rock-fluid properties of the matrix, fracture spacing, fracture permeability, fracture orientation and pressure of the system.
 - b) Create a two-dimensional single porosity model of a fracture with its fracture spacing undergoing waterflood with the properties obtained in (a). This model should be fine enough parallel and perpendicular to the fracture to represent it correctly.
 - c) Construct a one dimensional dual-porosity model using pseudo capillary pressure and match this model with the single porosity model already constructed. A sensitivity grid block size to the dual-porosity model should be also performed.
 - d) Use this dual porosity model for performing field scale simulation involving the area in study.
2. Dual-porosity model is not sensitive to the size of the numerical grid block.
3. De Swaan's equations can be used in field scale models.
4. Fluid viscosities play an important role in the countercurrent imbibition process, when higher the viscosities of the fluids the more time needed for recovering certain amount of the non-wetting phase.

NOMENCLATURE

Variables

B	= formation volume factor, L^3/L^3 [rcf/scf]
D	=depth of grid block, L , [ft]
f	=fractional flow,[fraction]
g	=fluid gradient, m/L^2t^2
i_w	=injection rate, L^3/t , [stb/D]
k	= permeability of the reservoir, L^2 , [md]
k_r	= relative permeability, L^2 , [md]
L	= matrix block dimension, L [ft]
N_p	=cumulative oil produce, L^3 ,[bbls]
p	= fluid pressure, m/Lt^2 , [psi]
q	= imbibition rate, L^3/t , [stb/D]
R	=recovered oil, L^3 , [bbls]
R_∞	=maximum movable oil recovery, L^3 , [bbls]
S	= saturation, [fraction]
t	= time, t , [days]
t_i	=time necessary to inject the fracture recoverable oil , t , [years]
t_{iN}	= time necessary to inject the matrix recoverable oil , t , [years]
T	= fluid transmissibility, $L^4 t/m$, [stb/d-psi]
V_b	=bulk volume of the reservoir, L^3 , [rcf]
Δx	=grid block dimension in x direction, L , [ft]
Δy	=grid block dimension in y direction, L , [ft]
Δz	=grid block dimension in z direction, L , [ft]
Δ	=finite-diference operator
Δ_t	=value at time $n+1$ minus value at time n

Subscripts

f	= fracture
g	= gas
i	= initial condition (usually refer to initial pressure)
L	= flow-path (high permeability layer)
ma	= matrix
u	= <i>unitary fracture length</i>
x	= x direction
y	= y direction
z	= z direction
α	=water and oil phase

Greek Symbols

ϕ	= porosity, [fraction]
ϕ_e	= effective porosity of fracture, [fraction]
σ	= shape factor, L^{-2} [ft^{-2}]
σ_1	= interfacial tension, [m/t^2]
ω	= weighting factor, [dimensionless]
λ	= fitting parameter, [t^{-1}]
τ_1	=the time necessary to produce 63% of recoverable oil, [t]
θ	=integration parameter

REFERENCES

1. De Swaan, A.: "Theory of Waterflooding in Fractured Reservoirs," paper SPE 5892 presented at the SPE-AIME Rocky Mountain Regional Meeting, Casper, Wyoming, 11-12 May, 1976.
2. Kleppe, J. and Morse, R.: "Oil Production from Fractured Reservoirs by Water Displacement," paper SPE 5084 presented at the 49th Annual Fall Meeting of the Society of Petroleum Engineers of AIME, Houston, 6-9 October, 1974.
3. Mattax, C. and KYTE, J.: "Imbibition Oil Recovery from Fractured, Water-Drive Reservoir," paper SPE 187 presented at the 36th Annual Fall Meeting, Dallas, Texas, 25 April, 1961.
4. Aronofsky, J., Masse, L., and Natanson, S.: "A Model for the Mechanism of Oil Recovery from the Porous Matrix due to Water Invasion in Fracture Reservoirs," *Trans.*, AIME (1958) 213, 17.
5. Kazemi, H., Gilman, J., and Elsharkawy, A.: "Analytical and Numerical Solution of Oil Recovery from Fractured Reservoirs with Empirical Transfer Functions," paper SPE 19849 presented at the 1989 SPE Annual Technical Conference and Exhibition. San Antonio, 8-11 October.
6. Warren, J., and Root, P.: "The Behavior of Naturally Fractured Reservoirs," paper SPE 426 presented at the Fall Meeting of the Society of Petroleum Engineers, Los Angeles, California, 21 March, 1962.

7. Gilman, J., and Kazemi, H.: "Improvements in Simulations of Naturally Fractured Reservoirs," paper SPE 10511 presented at the 1982 Reservoir Simulation Symposium, New Orleans, Jan. 31- Feb. 3.
8. Rangel, E., and Kovscek, A.: "Matrix-Fracture Transfer Functions for Partially and Completely Immersed Fractures," Geothermal Reservoir Engineering, Stanford, California, 27-29 Jan, 2003.
9. Thomas, L., Dixon T. and Pierson, R.: "Fractured Reservoir Simulation," paper SPE 9305 presented at the 1981 SPE Annual Technical Conference and Exhibition, San Antonio, 5-7 October.
10. Bourblaux, B. and Kalaydjian, F.: "Experimental Study of Cocurrent and Countercurrent Flows in Natural Porous Media," paper SPE 18283 presented at the 1988 SPE Annual Technical Conference and Exhibition, Houston, 2-5 October.
11. Gurpinar, O., and Kossack, C.: "Realistic Numerical Models for Fractured Reservoirs," paper SPE 59041 presented at the 2000 SPE International Petroleum Conference, Villa Hermoza, Mexico, 1-3 February.
12. Lee, J. and Kang, J.: "Oil Recovery in a Fracture of Variable Aperture with Countercurrent Imbibition," paper SPE 56416 presented at 1999 SPE Annual Technical Conference and Exhibition, Houston, 3-6 October.
13. Putra, E. and Schechter, D.S.: "Reservoir Simulation of Waterflood Pilot in Naturally Fractured Spraberry Trend Area," paper SPE 54336 presented at the 1999 SPE Asia Pacific Oil and Gas Conference and Exhibition, Jakarta, Indonesia, 20-22 April.

14. Zhou, D., Jia, L., and Kamath, J.: “An Investigation of Counter-Current Imbibition Processes in Diatomite,” paper SPE 68837 presented at the 2001 SPE Western Regional Meeting, Bakersfield, California, 26-30 March.
15. Bech, N., Jensen, O., and Nielsen, B.: “Modeling of Gravity-Drainage Processes: Analytic and Numerical Solutions,” paper SPE 18428 presented at the 1989 SPE Symposium on Reservoir Simulation, Houston, 6-8 February.
16. McDonald, A., Beckner, A., Chan, H., Jones, T., and Wooten, S.: “Some Important Considerations in the Simulation of Naturally Fractured Reservoirs,” paper SPE 21814 presented at the Rocky Mountain Regional Meeting, Denver, Colorado, 15-17 April, 1991.
17. Chowdhury, T., “Improving Dual Porosity Simulation of Waterflood Performance in the Naturally Fractured Spraberry Trend Area,” Master’s thesis, Texas A&M University, College Station, Texas (2002).
18. Lantz, R.: “Rigorous Calculation of Miscible Displacement Using Immiscible Reservoir Simulation,” paper SPE 2594 presented at SPE 44th Annual Fall Meeting, Denver, CO, 28 October, 1970.
19. Yamamoto, R., Ford, W., and Boubeguir, A.: “Compositional Reservoir Simulator for Fissured Systems- The Single- Block Model,” paper SPE 2666 presented at SPE 44th Annual Fall Meeting, Denver, CO, 28 October, 1971.
20. *CMG IMEX*, Vers. 2002, Computer Modeling Group, 1987-2002, Calgary, Canada.

21. Blair, P.: "Calculation of Oil Displacement by Countercurrent Water Imbibition," paper SPE 873 presented at the Fourth Biennial Secondary Recovery Recovery Symposium, Wichita Falls, Texas, 2-3 May, 1964.
22. Kazemi, H. and Zeman, P.: "Numerical Simulation of Water-Oil Flow in Naturally Fractured Reservoirs," paper SPE 5719 presented at the SPE-AIME Fourth Symposium on Numerical Simulation of Reservoir Performance, Los Angeles, California, 19-20 February, 1976.
23. Chen, J., Miller, M. and Sepehrnoori, K.: "Theoretical Investigation of Countercurrent Imbibition in Fractured Reservoir Matrix Blocks," paper SPE 29141 presented at the 13th SPE Symposium on Reservoir Simulation, San Antonio, 12-15 February, 1995.
24. Beckner, B., Firoozabadi, A. and Aziz, K.: "Modeling Transverse Imbibition in Double-Porosity Simulators," paper SPE 17414 presented at the SPE California Regional Meeting, Long Beach, California, 23-25 March, 1988.
25. Rossen, R. and Shen, E.: "Simulation of Gas /Oil Drainage and Water/Oil Imbibition in Naturally Fractured Reservoirs," paper SPE 16982 presented at 62nd Annual Technical Conference and Exhibition of the Society of Petroleum Engineers, Dallas, Texas, 27-30 September, 1987.

APPENDIX A
THE DATA FILE FOR THE DUAL-POROSITY MODEL USING
PSEUDO CAPILLARY PRESSURE CURVE

RESULTS SECTION INOUT

*INUNIT *FIELD

*OUTUNIT *FIELD

*INTERRUPT *RESTART-STOP

*RANGECHECK *ON

*XDR *ON

*MAXERROR 20

RESULTS XOFFSET 0.

RESULTS YOFFSET 0.

RESULTS ROTATION 0

RESULTS AXES-DIRECTIONS 1. -1. 1.

GRID VARI 4 1 1

KDIR DOWN

DUALPOR

SHAPE GK

TRANSFER 0

DI CON 353.333

DJ CON 3.16908

DK CON 10.

DTOP

4*7000.

**\$ RESULTS PROP NULL MATRIX Units: Dimensionless

**\$ RESULTS PROP Minimum Value: 1 Maximum Value: 1

**\$ 0 = NULL block, 1 = Active block

NULL MATRIX CON 1.

**\$ RESULTS PROP NULL FRACTURE Units: Dimensionless
 **\$ RESULTS PROP Minimum Value: 1 Maximum Value: 1
 **\$ 0 = NULL block, 1 = Active block
 NULL FRACTURE CON 1.

**\$ RESULTS PROP PINCHOUTARRAY Units: Dimensionless
 **\$ RESULTS PROP Minimum Value: 1 Maximum Value: 1
 **\$ 0 = PINCHED block, 1 = Active block
 PINCHOUTARRAY CON 1.
 RESULTS SECTION GRID

RESULTS SPEC 'Grid Thickness' MATRIX
 RESULTS SPEC SPECNOTCALCVAL 0
 RESULTS SPEC REGION 'Layer 1 - Whole layer'
 RESULTS SPEC REGIONTYPE 1
 RESULTS SPEC LAYERNUMB 1
 RESULTS SPEC PORTYPE 1
 RESULTS SPEC CON 10
 RESULTS SPEC STOP

RESULTS SPEC 'Grid Top' MATRIX
 RESULTS SPEC SPECNOTCALCVAL 0
 RESULTS SPEC REGION 'Layer 1 - Whole layer'
 RESULTS SPEC REGIONTYPE 1
 RESULTS SPEC LAYERNUMB 1
 RESULTS SPEC PORTYPE 1
 RESULTS SPEC CON 7000
 RESULTS SPEC STOP
 RESULTS PINCHOUT-VAL 0.0002 'ft'
 RESULTS SECTION NETPAY
 RESULTS SECTION NETGROSS
 RESULTS SECTION POR

RESULTS SPEC 'Porosity' MATRIX
 RESULTS SPEC SPECNOTCALCVAL 0
 RESULTS SPEC REGION 'Layer 1 - Whole layer'
 RESULTS SPEC REGIONTYPE 1
 RESULTS SPEC LAYERNUMB 1

RESULTS SPEC PORTYPE 1

RESULTS SPEC CON 0.1

RESULTS SPEC STOP

**\$ RESULTS PROP POR MATRIX Units: Dimensionless

**\$ RESULTS PROP Minimum Value: 0.05 Maximum Value: 0.1

POR MATRIX IVAR

0.05 2*0.1 0.05

**\$ RESULTS PROP POR FRACTURE Units: Dimensionless

**\$ RESULTS PROP Minimum Value: 0.000170396 Maximum Value: 0.000340793

POR FRACTURE IVAR

0.000170396 2*0.000340793 0.000170396

RESULTS SECTION PERMS

**\$ RESULTS PROP PERMI MATRIX Units: md

**\$ RESULTS PROP Minimum Value: 0.1 Maximum Value: 0.1

PERMI MATRIX CON 0.1

**\$ RESULTS PROP PERMI FRACTURE Units: md

**\$ RESULTS PROP Minimum Value: 17000 Maximum Value: 17000

PERMI FRACTURE CON 1.7E+04

**\$ RESULTS PROP PERMJ MATRIX Units: md

**\$ RESULTS PROP Minimum Value: 0.05 Maximum Value: 0.1

PERMJ MATRIX IVAR

0.05 2*0.1 0.05

**\$ RESULTS PROP PERMJ FRACTURE Units: md

**\$ RESULTS PROP Minimum Value: 8500 Maximum Value: 17000

PERMJ FRACTURE IVAR

8500. 2*1.7E+04 8500.

**\$ RESULTS PROP PERMK MATRIX Units: md

**\$ RESULTS PROP Minimum Value: 0.1 Maximum Value: 0.1

PERMK MATRIX CON 0.1

**\$ RESULTS PROP PERMK FRACTURE Units: md

**\$ RESULTS PROP Minimum Value: 17000 Maximum Value: 17000

PERMK FRACTURE CON 1.7E+04

RESULTS SECTION TRANS

RESULTS SECTION FRACS

**\$ RESULTS PROP DIFRAC Units: ft

**\$ RESULTS PROP Minimum Value: 0 Maximum Value: 0

DIFRAC CON 0

**\$ RESULTS PROP DJFRAC Units: ft

**\$ RESULTS PROP Minimum Value: 1.5845 Maximum Value: 1.5845

DJFRAC CON 1.5845

**\$ RESULTS PROP DKFRAC Units: ft

**\$ RESULTS PROP Minimum Value: 0 Maximum Value: 0

DKFRAC CON 0

RESULTS SECTION GRIDNONARRAYS

CPOR MATRIX 3.E-05

PRPOR MATRIX 2300.

CPOR FRACTURE 3.E-05

PRPOR FRACTURE 2300.

RESULTS SECTION VOLMOD

RESULTS SECTION SECTORLEASE

**\$ SECTORARRAY 'Fracture*2' FRACTURE Definition.

SECTORARRAY 'Fracture*2' FRACTURE ALL

4*1

**\$ SECTORARRAY 'Matrix*2' MATRIX Definition.

SECTORARRAY 'Matrix*2' MATRIX ALL

4*1

RESULTS SECTION ROCKCOMPACTION

RESULTS SECTION GRIDOTHER

RESULTS SECTION MODEL

MODEL *OILWATER

**\$ OilGas Table 'Table A'

*TRES 138.

*PVT *EG 1

** P	Rs	Bo	EG	VisO	VisG
14.7	3.37	1.0351	4.907985	5.9522	0.011977
27.05	4.65	1.0355	9.0445	5.8846	0.011985
39.4	6.	1.036	13.19303	5.8153	0.011993
51.76	7.41	1.0365	17.357	5.7448	0.012002
64.11	8.85	1.037	21.5297	5.6739	0.012012
76.46	10.35	1.0376	25.7145	5.6028	0.012023
88.82	11.88	1.0381	29.9148	5.5317	0.012034
101.17	13.44	1.0387	34.1239	5.4609	0.012045
113.52	15.03	1.0392	38.3452	5.3906	0.012057
125.88	16.66	1.0398	42.5822	5.3208	0.01207
138.23	18.31	1.0404	46.8279	5.2518	0.012082
150.59	19.99	1.041	51.0894	5.1835	0.012095
162.94	21.69	1.0416	55.3597	5.116	0.012108
175.29	23.41	1.0422	59.6423	5.0495	0.012122
187.65	25.16	1.0429	63.9408	4.9839	0.012135
200.	26.92	1.0435	68.2481	4.9193	0.012149
860.	139.92	1.0862	316.4086	2.7222	0.013156
1520.	273.72	1.1406	594.155	1.8192	0.014542
2180.	420.13	1.2038	877.637	1.3583	0.01628
2840.	575.92	1.2744	1135.694	1.084	0.018405
3500.	739.3	1.3517	1353.175	0.9036	0.020974

*DENSITY *OIL 55.

*DENSITY *GAS 0.0514

*DENSITY *WATER 66.2

*CO 2.151437E-05

*BWI 0.949

*CW 2.955295E-06

*REFPW 2300.

*VWI 0.516558

*CVW 0

RESULTS SECTION MODELARRAYS

RESULTS SECTION ROCKFLUID

*ROCKFLUID

*RPT 1

*SWT

0.320000	0.000000	1.000000	200.000000
0.371429	0.008000	0.452000	60.000000
0.422857	0.020000	0.292000	10.000000
0.474286	0.036000	0.180000	1.800000
0.525714	0.056000	0.124000	1.000000
0.577143	0.078000	0.068000	0.000000
0.628571	0.104000	0.0325173	0.000000
0.680000	0.138000	0.000000	0.000000

*RPT 2

*SWT

0.000000	0.000000	1.000000	8.000000
0.100000	0.100000	0.900000	0.100000
1.000000	1.000000	0.000000	0.000000

*KROIL *STONE2 *SWSG

RESULTS SECTION ROCKARRAYS

**\$ RESULTS PROP RTYPE MATRIX Units: Dimensionless

**\$ RESULTS PROP Minimum Value: 1 Maximum Value: 1

RTYPE MATRIX CON 1.

**\$ RESULTS PROP RTYPE FRACTURE Units: Dimensionless

**\$ RESULTS PROP Minimum Value: 2 Maximum Value: 2

RTYPE FRACTURE CON 2.

RESULTS SECTION INIT

*INITIAL

*USER_INPUT

**\$ Data for PVT Region 1

RESULTS SECTION INITARRAYS

RESULTS SPEC 'Pressure' MATRIX
 RESULTS SPEC SPECNOTCALCVAL 0
 RESULTS SPEC REGION 'Layer 1 - Whole layer'
 RESULTS SPEC REGIONTYPE 1
 RESULTS SPEC LAYERNUMB 1
 RESULTS SPEC PORTYPE 1
 RESULTS SPEC CON 2300
 RESULTS SPEC STOP

RESULTS SPEC 'Pressure' FRACTURE
 RESULTS SPEC SPECNOTCALCVAL 0
 RESULTS SPEC REGION 'Layer 1 - Whole layer'
 RESULTS SPEC REGIONTYPE 1
 RESULTS SPEC LAYERNUMB 1
 RESULTS SPEC PORTYPE 2
 RESULTS SPEC CON 2300
 RESULTS SPEC STOP

**\$ RESULTS PROP PRES MATRIX Units: psi
 **\$ RESULTS PROP Minimum Value: 2300 Maximum Value: 2300
 PRES MATRIX CON 2300.

**\$ RESULTS PROP PRES FRACTURE Units: psi
 **\$ RESULTS PROP Minimum Value: 2300 Maximum Value: 2300
 PRES FRACTURE CON 2300.

**\$ RESULTS PROP PB MATRIX Units: psi
 **\$ RESULTS PROP Minimum Value: 100 Maximum Value: 100
 PB MATRIX CON 100.

**\$ RESULTS PROP PB FRACTURE Units: psi
 **\$ RESULTS PROP Minimum Value: 100 Maximum Value: 100
 PB FRACTURE CON 100.

**\$ RESULTS PROP SO MATRIX Units: Dimensionless
 **\$ RESULTS PROP Minimum Value: 0.68 Maximum Value: 0.68

SO MATRIX CON 0.68

**\$ RESULTS PROP SO FRACTURE Units: Dimensionless

**\$ RESULTS PROP Minimum Value: 1 Maximum Value: 1

SO FRACTURE CON 1.

RESULTS SECTION NUMERICAL

*NUMERICAL

*DTMAX 30.

*DTMIN 1.E-10

*NEWTONCYC 800

*NORTH 400

*ITERMAX 200

*NCUTS 800

*NORM *PRESS 435.113

*NORM *PBUB 435.113

RESULTS SECTION NUMARRAYS

RESULTS SECTION GBKEYWORDS

RUN

DATE 1901 01 01.

WELL 1 'Injector'

INJECTOR MOBWEIGHT 'Injector'

INCOMP WATER

OPERATE MAX BHW 0.1 CONT

OPERATE MAX BHP 3100. CONT

GEOMETRY K 0.25 0.37 1. 0.

PERF GEOA 'Injector'

1 1 1 1. OPEN FLOW-FROM 'SURFACE'

WELL 2 'Producer'

PRODUCER 'Producer'

OPERATE MAX STL 0.11 CONT
OPERATE MIN BHP 500. CONT

GEOMETRY K 0.25 0.37 1. 0.
PERF GEOA 'Producer'
4 1 1 1. OPEN FLOW-TO 'SURFACE'

OPEN 'Injector'

OPEN 'Producer'

DATE 1901 02 01.

DATE 1901 03 01.

.

.

.

DATE 1940 01 01.

STOP

***** TERMINATE SIMULATION *****

RESULTS SECTION WELLDATA

RESULTS SECTION PERFS

VITA

Name: Christian Huapaya López

Permanent Address: Jr. Los Tulipanes 195
3 Barrio Obrero
Lima-31
Peru

Education: M.S., Petroleum Engineering
Texas A&M University, Petroleum Engineering Department
College Station, Texas, 2001

B.S., Petroleum Engineering
Universidad Nacional de Ingenieria
Lima, Peru, 1996

Experience: 2001 - Schlumberger (Anadrill), Talara, Peru
Petroleum Engineer

1998 – Perez Compañ, Peru
Petroleum Engineer

1997-1998 -Pluspetrol, Peru
Petroleum Engineer